CHAPTER 1 – INTRODUCTION AND THEORY OF THE FIELD GRADIENT BIREFRINGENCE EXPERIMENT

1.1 INTRODUCTION

In 1959 Buckingham developed a detailed theory [1] for an experiment that made it possible to determine the quadrupole moment of a molecule by measuring the birefringence induced in a medium by an external field gradient. The origin of this induced birefringence, first mentioned by Debye,[2] is the partial orientation of the molecular quadrupole moments by the field gradient, resulting in an anisotropic refractive index. Buckingham then proceeded with Disch to assemble the basic apparatus for such an experiment, from which they were able to obtain the first direct measurement of both the sign and magnitude of the quadrupole moment for carbon dioxide.[3]

The molar field gradient birefringence constant, ${}_{\mathrm{m}}Q$, is defined as [4]

$$ {}_{\mathrm{m}}Q = \frac{6n(3\varepsilon_{\mathrm{r}}+2)}{5\varepsilon_{\mathrm{r}}\left(n^2+2\right)^2} lim_{E_{xx}\to 0}\left(\frac{n_x - n_y}{E_{xx}}\right) V_{\mathrm{m}} \qquad (1.1) $$

where $n_x - n_y$ is the refractive index difference for light polarized parallel and perpendicular to the applied electric field gradient E_{xx}, n and ε_{r} are the isotropic refractive index and relative permittivity of the gas in the absence of the field and V_{m} is the molar volume.

A strict linear dependence of the molar field gradient birefringence constant upon gas density is not to be expected, as the anisotropy per molecule tends to be

increased by molecular interactions at higher pressures. Thus ${}_{\mathrm{m}}Q$ may, in principle, be described by the virial expression

$$ {}_{\mathrm{m}}Q = A_Q + \frac{B_Q}{V_{\mathrm{m}}} + \frac{C_Q}{V_{\mathrm{m}}^2} + \ldots \qquad (1.2) $$

in which A_Q, B_Q and C_Q are the first, second and third field gradient birefringence virial coefficients. B_Q and C_Q represent the deviation from A_Q due to interacting pairs and triplets of molecules respectively.

In this study no pressure dependence of the field gradient birefringence constant was observed for any of the molecules under investigation, hence the approximation ${}_{\mathrm{m}}Q = A_Q$ was made. Thus, with the effects of molecular interactions apparently being negligible, the derived quadrupole moments are applicable to isolated molecules.

1.2 MULTIPOLE MOMENTS

The forces between molecules have long been the subject of extensive investigations. For molecules that are far apart, where the separation is large compared to molecular dimensions, the interaction energy is determined by the permanent electric moments. These moments are used to characterize the molecular charge distribution and their subsequent interactions give rise to the electrostatic energy. An additional interaction, the induction energy, arises from the distortion of the electronic structures of neighbouring molecules by the electric fields produced by the permanent moments. Thus, to understand the nature of intermolecular forces, a detailed knowledge of molecular charge distributions and polarizabilities is required.

Consider a distribution of charges e_i at points (x_i, y_i, z_i) represented by the vectors r_i from an origin O as shown in Figure 1.1. The potential ϕ produced by a charge distribution at an arbitrary point P at a distance R, denoted by (x, y, z), from the origin, where $R > r_i$ for all i, is given by

$$\begin{aligned}\phi &= \sum_i \phi_i = (4\pi\varepsilon_0)^{-1} \sum_i e_i R_i^{-1} \\ &= (4\pi\varepsilon_0)^{-1} \sum_i e_i \left[(x - x_i)^2 + (y - y_i)^2 + (z - z_i)^2 \right]^{-\frac{1}{2}}\end{aligned} \tag{1.3}$$

where R_i is the distance between e_i and P.

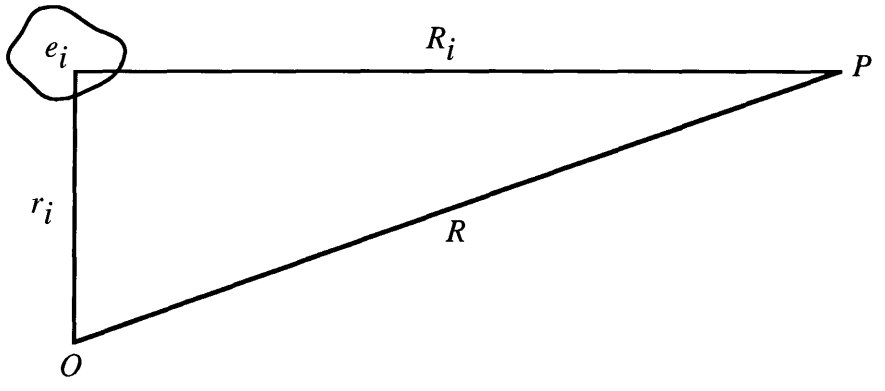

Figure 1.1 The position of the arbitrary point P relative to the charge distribution.

Expanding R_i^{-1} in terms of its derivatives with respect to $r_{i\alpha}$ at O one obtains

$$\phi = (4\pi\varepsilon_0)^{-1} \sum_i e_i \left[\frac{1}{R} + \left(\frac{\partial (1/R_i)}{\partial r_{i\alpha}} \right)_0 r_{i\alpha} + \frac{1}{2} \left(\frac{\partial^2 (1/R_i)}{\partial r_{i\alpha} \partial r_{i\beta}} \right)_0 r_{i\alpha} r_{i\beta} + \frac{1}{6} \left(\frac{\partial^3 (1/R_i)}{\partial r_{i\alpha} \partial r_{i\beta} \partial r_{i\gamma}} \right)_0 r_{i\alpha} r_{i\beta} r_{i\gamma} + \cdots \right]$$

$$= (4\pi\varepsilon_0)^{-1}\left[\frac{q}{R} + \frac{\mu_\alpha R_\alpha}{R^3} + \frac{Q_{\alpha\beta}}{2R^5}\left(3R_\alpha R_\beta - R^2\delta_{\alpha\beta}\right) + \right.$$
$$\left. \frac{R_{\alpha\beta\gamma}}{2R^7}\left\{5R_\alpha R_\beta R_\gamma - R^2\left(R_\alpha\delta_{\beta\gamma} + R_\beta\delta_{\gamma\alpha} + R_\gamma\delta_{\alpha\beta}\right)\right\} + \ \ldots\right] \tag{1.4}$$

in which $\delta_{\alpha\beta}$ is the substitution tensor and

$$\begin{aligned} q &= \sum_i e_i \\ \mu_\alpha &= \sum_i e_i r_{i_\alpha} \\ Q_{\alpha\beta} &= \sum_i e_i r_{i_\alpha} r_{i_\beta} \\ R_{\alpha\beta\gamma} &= \sum_i e_i r_{i_\alpha} r_{i_\beta} r_{i_\gamma} \end{aligned} \tag{1.5}$$

The above moments of charge q, μ_α, $Q_{\alpha\beta}$ and $R_{\alpha\beta\gamma}$ refer to the total charge (zeroth moment), the electric dipole moment (first moment), the quadrupole moment (second moment) and the octopole moment (third moment), respectively.

Apart from describing the total molecular charge distribution, the multipole moments also determine the potential energy of interaction of the charge distribution with an external field. For a distribution of charges e_i in a potential ϕ_i at points r_i relative to the origin, the energy of interaction U is

$$U = \sum_i e_i\phi_i \tag{1.6}$$

Expanding ϕ_i in a Taylor series about the origin yields

$$U = \sum_i e_i\left\{\phi_0 + \left(\frac{\partial\phi}{\partial r_\alpha}\right)_0 r_{i_\alpha} + \frac{1}{2}\left(\frac{\partial^2\phi}{\partial r_\alpha \partial r_\beta}\right)_0 r_{i_\alpha} r_{i_\beta} + \frac{1}{6}\left(\frac{\partial^3\phi}{\partial r_\alpha \partial r_\beta \partial r_\gamma}\right)_0 r_{i_\alpha} r_{i_\beta} r_{i_\gamma} + \ \ldots\right\}$$

$$= q\phi_0 - \mu_\alpha E_\alpha - \frac{1}{2} Q_{\alpha\beta} E_{\alpha\beta} - \frac{1}{6} R_{\alpha\beta\gamma} E_{\alpha\beta\gamma} - \ldots \tag{1.7}$$

and $E_\alpha = -\left(\frac{\partial \phi}{\partial r_\alpha}\right)_0$ and $E_{\alpha\beta} = -\left(\frac{\partial^2 \phi}{\partial r_\alpha \partial r_\beta}\right)_0$ are the α and $\alpha\beta$ components of the external field and field gradient at the origin.

Some authors use the above primitive quadrupole moment, $Q_{\alpha\beta} = \sum_i e_i r_{i\alpha} r_{i\beta}$, to define the quadrupole moment. However a more common definition, which describes departures from spherical symmetry, is the traceless quadrupole moment given by [5]

$$\begin{aligned} \Theta_{\alpha\beta} &= \frac{1}{2}\left(3Q_{\alpha\beta} - Q_{\gamma\gamma}\delta_{\alpha\beta}\right) \\ &= \frac{1}{2}\sum_i e_i \left(3r_{i\alpha} r_{i\beta} - r_i^2 \delta_{\alpha\beta}\right) \end{aligned} \tag{1.8}$$

The latter is considered to be the better definition as $\Theta_{\alpha\beta}$ vanishes for spherically symmetric charge distributions.

Treating the octopole moment in a similar manner (which is zero for a spherical distribution of charge), the following expression is obtained

$$\begin{aligned} \Omega_{\alpha\beta\gamma} &= \frac{1}{2}\left(5R_{\alpha\beta\gamma} - R_{\alpha\delta\delta}\delta_{\beta\gamma} - R_{\beta\delta\delta}\delta_{\gamma\alpha} - R_{\gamma\delta\delta}\delta_{\alpha\beta}\right) \\ &= \frac{1}{2}\sum_i e_i \left\{5r_{i\alpha} r_{i\beta} r_{i\gamma} - r_i^2 \left(r_{i\alpha}\delta_{\beta\gamma} + r_{i\beta}\delta_{\alpha\gamma} + r_{i\gamma}\delta_{\alpha\beta}\right)\right\} \end{aligned} \tag{1.9}$$

By Laplace's equation, $E_{\alpha\alpha} = E_{xx} + E_{yy} + E_{zz} = 0$, and with the above definitions for the quadrupole moment and octopole moment, equation (1.7) simplifies to

$$U = q\phi_0 - \mu_\alpha E_\alpha - \frac{1}{3}\Theta_{\alpha\beta} E_{\alpha\beta} - \frac{1}{15}\Omega_{\alpha\beta\gamma} E_{\alpha\beta\gamma} - \ldots \tag{1.10}$$

As the quadrupole moment is a symmetric second rank tensor, it is possible to find three mutually perpendicular molecule fixed axes such that $\Theta_{\alpha\beta} = 0$ if $\alpha \neq \beta$. Consequently there are three principal quadrupole moments Θ_{xx}, Θ_{yy} and Θ_{zz}. However, from equation (1.8), $\Theta_{\alpha\alpha} = 0$ and only two are independent and therefore necessary to describe the interaction of the system with a field gradient.

If the charge distribution is symmetric about the z-axis

$$\Theta_{xx} = \Theta_{yy} = -\frac{1}{2}\Theta_{zz} = -\frac{1}{2}\Theta \tag{1.11}$$

To determine the effect on the quadrupole moment of a change of origin, consider moving O to O' at a distance r' from O. The quadrupole moment Θ' relative to the new origin O' is given by

$$\begin{aligned}\Theta'_{\alpha\beta} &= \frac{1}{2}\sum_i e_i\left\{3r'_{i\alpha}r'_{i\beta} - \left(r'_i\right)^2\delta_{\alpha\beta}\right\} \\ &= \Theta_{\alpha\beta} - \frac{3}{2}\mu_\alpha r'_\beta - \frac{3}{2}\mu_\beta r'_\alpha + \mu_\gamma r'_\gamma\delta_{\alpha\beta} + \frac{1}{2}q\left\{3r'_\alpha r'_\beta - \left(r'\right)^2\delta_{\alpha\beta}\right\}\end{aligned} \tag{1.12}$$

Hence, the quadrupole moment is independent of the choice of origin only if both q and μ_α are zero. This follows the well established rule that only the first non-zero electric multipole moment is independent of the origin. Thus for a dipolar molecule, the quadrupole moment varies depending on the location of the origin. This will be discussed further in section 1.5.3.

1.3 THE POLARIZABILITY AND RAYLEIGH LIGHT SCATTERING

The polarizability tensor, $\alpha_{\alpha\beta}$, describes the electric dipole moment induced in a molecule by an electric field that arises from the distortion of the mean position of the

electrons and nuclei by the field. It has three principal components, α_{xx}, α_{yy} and α_{zz}, from which the mean polarizability, α, is defined as

$$\alpha = \frac{1}{3}\alpha_{\alpha\alpha} = \frac{1}{3}\left(\alpha_{xx} + \alpha_{yy} + \alpha_{zz}\right) \tag{1.13}$$

where *x, y, z* denote the principal axes.

For molecules with an axis of 3-fold or higher symmetry (chosen to be the *z*-axis), $\alpha_{xx} = \alpha_{yy}$, and the above equation simplifies to

$$\alpha = \frac{1}{3}(\alpha_{\parallel} + 2\alpha_{\perp}) \tag{1.14}$$

in which $\alpha_{\parallel}$ and $\alpha_{\perp}$ are the polarizabilities along and at right angles to the symmetry axis, respectively.

The anisotropy, κ, of the polarizability tensor, $\alpha_{\alpha\beta}$, is defined by [6]

$$\kappa^2 = \frac{3\alpha_{\alpha\beta}\alpha_{\alpha\beta} - \alpha_{\alpha\alpha}\alpha_{\beta\beta}}{2\alpha_{\alpha\alpha}\alpha_{\beta\beta}} \tag{1.15}$$

If a 3-fold or higher-order axis of symmetry is present in the molecule, equation (1.15) reduces to

$$\kappa = \frac{\Delta\alpha}{3\alpha} \tag{1.16}$$

where $\Delta\alpha = \alpha_{\parallel} - \alpha_{\perp}$ is the polarizability anisotropy. Values of $\Delta\alpha$ are commonly obtained from the depolarization ratio, ρ_0, for Rayleigh scattered light.

For a light beam, vertically polarized to the scattering plane, incident on a medium, the depolarization ratio, ρ_0, for Rayleigh scattering at 90° to the incident beam is defined as [6]

$$\rho_0 = \frac{I_h}{I_v} \tag{1.17}$$

in which I_h and I_v are the measured intensities of the scattered light that passes through an analyzer aligned perpendicular and parallel to the electric vector of the incident light, respectively.

For a gas consisting of randomly orientated molecules in the absence of electronic angular momentum and magnetic fields, the depolarization ratio, ρ_0, is given by the classical relation [6]

$$\rho_0 = \frac{3\kappa^2}{5+4\kappa^2} \tag{1.18}$$

where κ is the anisotropy of the polarizability tensor, $\alpha_{\alpha\beta}$.

Equation (1.18) is applicable to all but the lightest molecules, provided the whole of the rotational Raman spectrum is included and the vibrational Raman scattering is excluded in the measurement of ρ_0.

1.4 THE QUADRUPOLE HYPERPOLARIZABILITY

The hyperpolarizability, $B_{\alpha\beta:\gamma\delta}$, consists of three terms which arise from the distortion of the molecule by the external field gradient [7]

$$\frac{15}{2}B = B_{\alpha\beta:\alpha\beta} - \beta_{\alpha\beta:\alpha\beta} - \frac{5}{\omega}\varepsilon_{\alpha\beta\gamma}J_{\alpha\beta\gamma} \tag{1.19}$$

where $\varepsilon_{\alpha\beta\gamma}$ is the alternating tensor and ω is the angular frequency of the light. The hyperpolarizability tensors $B_{\alpha\beta:\alpha\beta}$, $\beta_{\alpha\beta:\alpha\beta}$ and $J_{\alpha\beta\gamma}$ are defined elsewhere.[7]

At frequencies well below the first electronic excitation frequency of the molecule, $B_{\alpha\beta:\alpha\beta} = \beta_{\alpha\beta:\alpha\beta}$, and the hyperpolarizability simplifies to its lowest frequency limit

$$\left(\frac{15}{2}B\right)_{\omega=0} = -\left(\frac{5}{\omega}\varepsilon_{\alpha\beta\gamma}J_{\alpha\beta\gamma}\right)_{\omega=0} \tag{1.20}$$

1.5 THEORIES OF THE FIELD GRADIENT BIREFRINGENCE EXPERIMENT

1.5.1 Classical Theory

The approach used by Buckingham [1] in deriving the classical expression for the field gradient birefringence effect is similar to the one presented by Buckingham and Pople for the electrooptical Kerr effect [8] and the magnetooptical Cotton-Mouton effect.[9]

For an uncharged molecule in an external potential ϕ, having a configuration τ (representing the position and orientation of the molecule), the expression for its energy, U, can be written as

$$U(\tau,\phi) = U^{(0)} - \mu_\alpha E_\alpha - \frac{1}{2}\alpha_{\alpha\beta}E_\alpha E_\beta - \frac{1}{6}\beta_{\alpha\beta\gamma}E_\alpha E_\beta E_\gamma - \frac{1}{24}\gamma_{\alpha\beta\gamma\delta}E_\alpha E_\beta E_\gamma E_\delta$$

$$-\frac{1}{3}\Theta_{\alpha\beta}E_{\alpha\beta} - \frac{1}{3}A_{\alpha:\beta\gamma}E_\alpha E_{\beta\gamma} - \frac{1}{6}B_{\alpha\beta:\gamma\delta}E_\alpha E_\beta E_{\gamma\delta} - \ldots \tag{1.21}$$

where μ_α and $\Theta_{\alpha\beta}$ are the permanent dipole and quadrupole moments of the molecule. The higher rank tensors are the polarizabilities describing the distortion of the molecule by E_α and $E_{\alpha\beta}$.

The differential polarizability, $\Pi_{\alpha\beta}$, is defined as the increase in dipole moment per unit increase in field such that

$$\begin{aligned}\Pi_{\alpha\beta} &= \frac{-\partial^2 U}{\partial E_\alpha \partial E_\beta} \\ &= \alpha_{\alpha\beta} + \beta_{\alpha\beta\gamma}E_\gamma + \frac{1}{3}B_{\alpha\beta:\gamma\delta}E_{\gamma\delta} + \ldots\end{aligned} \tag{1.22}$$

The symmetry of the two wire field gradient cell ensures that on the cell axis $E_\alpha = 0$, $E_{xx} = -E_{yy}$. The anisotropy in the refractive index of a gas for a beam of light travelling along the axis of the cell with electric vectors in the x and y direction is

$$n_x - n_y = \frac{N_A \overline{\Pi}}{2\varepsilon_0 V_m} \tag{1.23}$$

where $\overline{\Pi}$ is the mean value of the scalar Π defined by

$$\Pi(\tau, \phi) = \Pi_{\alpha\beta}\left(e_\alpha^{\parallel} e_\beta^{\parallel} - e_\alpha^{\perp} e_\beta^{\perp}\right) \tag{1.24}$$

in which $e_\alpha^{\parallel}$ and $e_\alpha^{\perp}$ are unit vectors parallel and perpendicular to the electric field.

Expanding $\overline{\Pi}$ as a power series in the field and field gradient leads to the expression

$$\overline{\Pi} = \left(\frac{\partial \overline{\Pi}}{\partial E_{xx}}\right)_{\phi=0} E_{xx} + \frac{1}{2}\left(\frac{\partial^2 \overline{\Pi}}{\partial E^2}\right)_{\phi=0} E^2 + \frac{1}{6}\left(\frac{\partial^3 \overline{\Pi}}{\partial E_{xx}^3}\right)_{\phi=0} E_{xx}^3 + \ldots \tag{1.25}$$

in which $\overline{\Pi}$ is an odd function of E_{xx} and an even one of E. For all moderate field gradients ($E_{xx} < 10^9$ V m^{-2}), the anisotropy induced in the gas can be described by the first term in E_{xx}, as $E = 0$ along the z-axis and all the other terms make a negligible contribution.

Hence

$$\begin{aligned}\overline{\Pi} &= \left(\frac{\partial\overline{\Pi}}{\partial E_{xx}}\right)_{\phi=0} E_{xx} \\ &= E_{xx}\left\{\left\langle\frac{\partial\Pi}{\partial E_{xx}}\right\rangle - \left(\frac{1}{kT}\right)\left\langle\Pi\frac{\partial U}{\partial E_{xx}}\right\rangle\right\}\end{aligned} \tag{1.26}$$

where the angular brackets indicate an average over all τ when $\phi = 0$.

From equations (1.21), (1.22) and (1.24)

$$\left\langle\frac{\partial\Pi}{\partial E_{xx}}\right\rangle = \frac{6}{45}B_{\alpha\beta:\alpha\beta} \tag{1.27}$$

$$\left\langle\Pi\left(\frac{\partial U}{\partial E_{xx}}\right)\right\rangle = -\frac{6}{45}\alpha_{\alpha\beta}\Theta_{\alpha\beta} \tag{1.28}$$

so that (1.23), (1.25), (1.27) and (1.28) lead to the result

$$n_x - n_y = \frac{N_A E_{xx}}{15\varepsilon_0 V_m}\left\{B_{\alpha\beta:\alpha\beta} + \frac{\alpha_{\alpha\beta}\Theta_{\alpha\beta}}{kT}\right\} \tag{1.29}$$

For molecules with a 3-fold or higher-order axis of symmetry

$$n_x - n_y = \frac{N_A E_{xx}}{15\varepsilon_0 V_m}\left\{\frac{15}{2}B + \frac{\Delta\alpha\Theta}{kT}\right\} \tag{1.30}$$

where $\Delta\alpha = \alpha_{zz} - \alpha_{xx}$ and the scalar quantity $B_{\alpha\beta:\alpha\beta}$ is written as $\frac{15}{2}B$.[10]

If the molecule is spherically symmetric $\Theta = 0$ and

$$n_x - n_y = \frac{N_A E_{xx}}{15\varepsilon_0 V_m}\left(\frac{15}{2}B\right) \tag{1.31}$$

In this particular case, the induced birefringence has been shown to be proportional to the Verdet constant of the gas.[11]

1.5.2 Quantum Mechanical Theory

Quantum corrections to the classical formula relating the induced birefringence to the quadrupole moment have been investigated by Buckingham and Pariseau [12] for a non-dipolar molecule. The quantum mechanical expression for a linear molecule is given by

$$n_x - n_y = \frac{N_A E_{xx}}{15\varepsilon_0 V_m}\left\{\frac{15}{2}B' + \frac{\Delta\alpha\Theta}{kT}f(t)\right\} \tag{1.32}$$

$$f(t) = 1 - \sigma_0 + \frac{8}{15}\sigma_0^2 - \ldots \tag{1.33}$$

where B' differs from B because of centrifugal distortion, $\sigma_0 = hcB_0/kT$ and B_0 is the rotational constant. For H_2 at room temperature $f(t)$ is 0.75 while for CO_2 $f(t)$ is 0.998. Hence, the effects of quantization of the rotational motion are negligible in most

cases and can be ignored except in the case of very small molecules with large rotational constants.

1.5.3 Dipolar Molecules

For a dipolar molecule, the electric quadrupole moment depends upon the molecular origin from which it is measured. Originally, it was suggested that the field gradient birefringence technique gave the quadrupole moment relative to the centre of mass [1] but this has been shown to be incorrect for dipolar molecules. In any given gas, the optical anisotropy induced by an electric field gradient depends only on the electric properties of the molecules and on their configurational distribution in the field. For a set of molecules in equilibrium, the configurational distribution is determined solely by their potential energy. To a high degree of approximation, these properties are the same for isotopically distinct molecules, hence the field gradient birefringence effect must give identical experimental readings for isotopically distinct but chemically identical species. However, as the centre of mass quadrupole moment is dependent on the nuclear masses, different results would be obtained for isotopic species. Thus the field gradient birefringence effect cannot give the quadrupole moment relative to the centre of mass.

As dipolar molecules experience a force in the field gradient and this enhances the contribution to the anisotropy of the refractive index, equation (1.29) cannot be used to evaluate the quadrupole moment for a dipolar molecule.

The first theory for the treatment of dipolar molecules was put forward by Buckingham and Longuet-Higgins.[7] Their expression relating the induced birefringence to the quadrupole moment is given below

$$n_x - n_y = \frac{N_A E_{xx}}{15\varepsilon_0 V_m}\left\{\frac{15}{2}B + \frac{1}{kT}\left[\Delta\alpha\Theta - \mu\left(A_{\parallel} + 2A_{\perp} + \frac{10}{\omega}G'\right)\right]\right\} \tag{1.34}$$

where the origin of the quadrupole moment is defined relative to a point referred to as the effective quadrupole centre at which $A_{\parallel} + 2A_{\perp} + \frac{10}{\omega}G' = 0$. The higher polarizabilities A and G' describe the electric dipole induced by the field gradient and the time-dependent magnetic field associated with the electromagnetic wave. The position of the effective quadrupole centre depends on the angular frequency of the light used to measure the birefringence, but is considered to be independent of the nuclear masses. This approach has been used by previous workers to obtain quadrupole moments for several dipolar molecules.[13,14,15]

However, Imrie and Raab[16] have suggested that the above expression is inapplicable to the field gradient birefringence experiment in that the theory describes birefringence as an incoherent phenomenon whereas birefringence is a coherent property. In turn, they derive an expression for the birefringence induced by an electric field gradient in dipolar molecules using a theory based on Maxwell's equations, satisfying the requirement that the expression be independent of the molecular origin. Their expression for a linear molecule is given by

$$n_x - n_y = \frac{N_A E_{xx}}{15\varepsilon_0 V_m}\left\{\frac{15}{2}B + \frac{1}{kT}\left[Q\Delta\alpha - \frac{1}{2}\mu\left(2a_1 + a_2 + 3a_3 + \frac{10}{\omega}G'\right)\right]\right\} \tag{1.35}$$

where a and G' are higher polarizabilities defined elsewhere,[16] and $\mu = \mu_z$; $Q = Q_{zz} - Q_{xx}$; $\Delta\alpha = \alpha_{zz} - \alpha_{xx}$; $a_1 = a_{zzz}$; $a_2 = a_{xxz} = a_{yyz}$; $a_3 = a_{zxx} = a_{zyy}$ and $G' = G'_{xy} = -G'_{yx}$.

The quadrupole moment, Q, in the above expression refers to the primitive quadrupole moment defined earlier in equation (1.5). Similarly, the origin of the quadrupole moment is defined relative to the effective quadrupole centre. For a linear

molecule it is easily shown that $Q = \Theta_{zz}$. Results obtained in the present work will be reported using the traceless definition of the molecular quadrupole moment, thereby enabling a direct comparison with other values reported in the literature.

Although both of the above methods yield the same value for the effective quadrupole moment, a discrepancy arises between the two theories when calculating the position of the effective quadrupole centre.

The effective quadrupole centre may be regarded as the point at which the first moment of the polarizability anisotropy vanishes. If the effective quadrupole centre is a distance Z from the centre of mass in the direction of the dipole moment μ, then the centre of mass quadrupole moment, Θ_{CM}, is related to the effective quadrupole moment, Θ_{EQC}, by the expression

$$\Theta_{CM} - \Theta_{EQC} = 2\mu Z \tag{1.36}$$

Hence, a value of Z can be obtained from a knowledge of both Θ_{CM} and Θ_{EQC}, thus enabling the position of the effective quadrupole centre to be determined. Also, by combining Z with the polarizability anisotropy, information on the higher polarizabilities, a and G, can be obtained using the following relation [13]

$$\left(2a_1 + a_2 + 3a_3 + \frac{10}{\omega}G'\right) = 2\Delta\alpha Z \tag{1.37}$$

1.5.4 The Molar Field Gradient Birefringence Constant

Results from previous studies of the Kerr effect and Cotton-Mouton effect have been reported in terms of the molar Kerr constant[17-19] and molar Cotton-Mouton

constant.[20-22] An analogous treatment for the field gradient birefringence experiment will be used throughout this work, where the results will be reported in terms of the molar field gradient birefringence constant.

The molar field gradient birefringence constant, ${}_{\mathrm{m}}\underline{Q}$, defined earlier in equation (1.1) in terms of the experimental observables, simplifies when dealing with low gas pressures. For a linear molecule, the relationship between the observed birefringence and the fundamental electric properties is given by

$$\begin{aligned} {}_{\mathrm{m}}Q &= \frac{2}{3}\frac{(n_x - n_y)V_{\mathrm{m}}}{E_{xx}} \\ &= \frac{2N_{\mathrm{A}}}{45\varepsilon_0}\left\{\frac{15}{2}B + \frac{1}{kT}\left[\Theta\Delta\alpha - \frac{1}{2}\mu\left(2a_1 + a_2 + 3a_3 + \frac{10}{\omega}G'\right)\right]\right\} \end{aligned} \tag{1.38}$$

in which the birefringence, $n_x - n_y$, is given by equation (1.35).

1.6 ALTERNATIVE METHODS FOR DETERMINING QUADRUPOLE MOMENTS

Much of the early information that was reported on molecular quadrupole moments was provided by the study of molecular interactions. As many of the methods used are indirect and depend on assumptions related to the intermolecular force-field, the values obtained are known to be uncertain. Several of these methods, some more reliable than others, are discussed below.

1.6.1 Second Virial Coefficients [5,23–26]

Experiments have shown that interactions between gas molecules lead to deviations from ideal gas behaviour. This deviation is given by

$$\frac{pV}{RT} = 1 + \frac{B(T)}{V_m} + \frac{C(T)}{V_m^2} + \ldots \tag{1.39}$$

where B and C are the second and third density virial coefficients respectively. For non-dipolar molecules, if the expression for B in terms of the interaction potential energy, U, is known, an estimate of the quadrupole moment (the leading parameter of this potential) can be made. This is achieved by choosing an appropriate model of the potential and adjusting the value of Θ until this value of B agrees with the experimentally determined value.

Quadrupole moments obtained from this method, when compared to more recent results, have proved unreliable.

1.6.2 Dielectric Constant Method [5,23,27–29]

The dielectric behaviour of a gas can be described by the virial expansion of the Clausius-Mossotti equation

$$\frac{\varepsilon_r - 1}{\varepsilon_r + 2} V_m = A_\varepsilon + \frac{B_\varepsilon}{V_m} + \frac{C_\varepsilon}{V_m^2} + \ldots \tag{1.40}$$

where ε_r is the static value of the dielectric constant, and A_ε, B_ε and C_ε are the first, second and third virial coefficients respectively, representing the contributions from single molecules, pairs and triplets.

Only the dielectric second virial coefficient, B_ε, is of particular interest in this case. Buckingham and Pople [27] used classical statistical theory to express this as

$$B_\varepsilon = B_{IND} + B_{OR} \tag{1.41}$$

where B_{IND} results from the interaction of the dipole moments induced by the external field and B_{OR} accounts for the orientation in the external field of moments induced in one molecule of the pair by the other.

In order to determine the quadrupole moment for a given molecule it is necessary to separate B_{IND} and B_{OR}, with the latter term being dependent on Θ. This can be achieved by the Lorenz - Lorentz equation

$$\frac{n^2-1}{n^2+2}V_m = A_R + \frac{B_R}{V_m} + \frac{C_R}{V_m^2} + \ldots \tag{1.42}$$

where A_R, B_R and C_R are the first, second and third refractivity virial coefficients and n is the refractive index. Thus, by measuring the variation of refractive index with density, and because orientation effects do not contribute at optical frequencies, the approximation $B_{IND} = B_R$ can be made and B_{OR} can be calculated, from which a value of the quadrupole moment can be obtained.[28,29]

Again, this method involves many assumptions about intermolecular forces and therefore the results can be uncertain.

1.6.3 Collision Induced Absorption [5,30–33]

Non-dipolar molecules when placed under high pressures can acquire dipole moments induced by the intermolecular forces in clusters of two or more interacting molecules. These induced dipole moments arise from short-range overlap forces and the resultant polarization of one molecule by the quadrupole field of the other. Such dipole moments give rise to induced vibrational, rotational and translational transitions

which can be studied using infrared absorption. In these experiments it is the translational-rotational transitions, appearing as broad bands in the far infrared, that are of concern here.

From the resulting spectra, one obtains an experimentally determined absorption coefficient defined by

$$\varphi = \int A(\omega) d\omega \tag{1.43}$$

in which $A(\omega)$ is the absorption coefficient, calculated by integrating over the complete rotational-translational band.

Expanding φ as a function of density, Poll and Van Kranendonk [30] obtained

$$\varphi = \frac{\varphi_1}{V_m^2} + \frac{\varphi_2}{V_m^3} + \ldots \tag{1.44}$$

where φ_1 and φ_2 are respectively the rotational-translational absorption coefficients due to collisions between pairs and triplets of molecules.

Assuming that the contribution to the induced dipole moments arises from the quadrupolar induction and ignoring the overlap forces, the quadrupole moment can be obtained from φ_1.[32,33]

1.6.4 Magnetic Anisotropy Method [5,23,34–37]

The rotational Zeeman effect arises from the interactions of a freely rotating molecule with zero orbital and spin-electronic angular momentum in the ground electronic state with an external magnetic field.

The first interaction involves the molecular magnetic-moment tensor (molecular g value) and leads to the first-order Zeeman effect. A second interaction involves the response of the electrons in the system to the external magnetic field. This leads to the second-order Zeeman effect, from which a measurement of the magnetic anisotropy, $\Delta\chi$, can be obtained. Knowing both the molecular g value and the magnetic anisotropy leads directly to an experimental determination of the diagonal elements of the molecular quadrupole moment tensor in the principal inertial axis system of the molecule.[35] Thus for all molecules, the values of Θ are given relative to the centre of mass Θ_{CM}.

The expression for the molecular quadrupole moment of a planar axially symmetric molecule is given by [37]

$$\Theta = -\frac{e}{M_p}\left(g_{\|}I_{\|} - g_{\perp}I_{\perp}\right) - \frac{4m}{e}\Delta\chi \qquad (1.45)$$

where $\Delta\chi = \chi_{\|} - \chi_{\perp}$ is the magnetic anisotropy, $I_{\|}$ and $I_{\perp}$ are the principal moments of inertia, M_p is the proton mass, m is the electron mass, and e the elementary charge.

For a linear molecule, the above expression reduces to

$$\Theta = \frac{eg_{\perp}I}{M_p} - \frac{4m}{e}\Delta\chi \qquad (1.46)$$

This method has been applied to a variety of molecules, enabling both the sign and magnitude of the molecular quadrupole moment to be calculated.

When dealing with larger molecules, because the two terms involving $\Delta\chi$ and $g_{\perp}$ generally have opposite signs and increase in magnitude as the size of the molecule

increases, the small difference between the two terms becomes somewhat uncertain, therefore making the quadrupole moment unreliable.

1.6.5 Other Methods

Several other methods have been used to approximate the molecular quadrupole moment. These include ion-molecule scattering experiments,[38] nuclear spin relaxation times[39] and molecular orbital calculations.[40-42] This last method is proving to be quite successful when large basis sets are used and the effects of electron correlation and vibrational averaging are considered.

1.7 DISCUSSION

Although the field gradient birefringence experiment is the most direct and precise method available for determining molecular quadrupole moments, only a few molecules have been studied using this technique.[3,13,14,15,43-49]

The size of the induced birefringence from the field gradient technique is very small when compared to other birefringence experiments such as the Kerr effect and the Cotton-Mouton effect, and consequently it has proved hard to measure accurately. In order to determine the quadrupole moment, measurements should be performed over a range of temperatures to separate the contribution from the temperature-independent term that contains the quadrupole hyperpolarizability. However, as the size of the effect decreases linearly as the temperature increases, the experiment becomes even more difficult. To avoid these practical difficulties, much of the early work has consisted of measurements performed at single temperatures of substances in the vapour phase [3,13,14,15,43-45] or as dilute solutions.[46-49] Results from these

measurements rely on the validity of the assumptions regarding the contribution of the quadrupole hyperpolarizability and also, in the case of the solution-phase measurements, any solvent effects.

The intention of the present work was to measure the molecular quadrupole moments of a number of molecules using the field gradient birefringence experiment. These molecules included carbon dioxide, carbonyl sulfide, carbon disulfide, benzene, hexafluorobenzene, ethane, hexafluoroethane, cyclopropane, cyclohexane, nitrogen, acetylene, methylacetylene and dimethylacetylene. Unfortunately, due to the very small effect, it was impossible to obtain reliable results for carbonyl sulfide, hexafluoroethane and cyclohexane. Temperature-dependence studies were carried out on most of the remaining molecules with the exception of the acetylenes.

Apart from one previous study by Battaglia *et al* on carbon dioxide,[45] this is the first comprehensive investigation of the temperature dependence of the field gradient birefringence effect, in which a wide variety of molecules will be studied. It was hoped that this would provide a better understanding of the contribution of the hyperpolarizability term in the field gradient birefringence effect.

The following chapters give a detailed description of the equipment that was built to perform the field gradient induced birefringence measurements. The results and conclusions for the molecules mentioned above are then presented. Where possible, the results from this study are compared with previous values that have been reported in the literature.

1.8 REFERENCES

1. A.D. Buckingham, *J. Chem. Phys.*, **30**, 1580 (1959).

2. P. Debye, *Phys. Z.*, **22**, 302 (1921).

3. A.D. Buckingham and R.L. Disch, *Proc. Roy. Soc. A*, **273**, 275 (1963).

4. J. Vrbancich and G.L.D. Ritchie, *J. Chem. Soc. Faraday Trans. II*, **76**, 648 (1980).

5. A.D. Buckingham, *Quart. Rev.*, **13**, 183 (1959).

6. N.J. Bridge and A.D. Buckingham, *Proc. Roy. Soc. A*, **295**, 334 (1966).

7. A.D. Buckingham and H.C. Longuet-Higgins, *Molec. Phys.*, **14**, 63 (1968).

8. A.D. Buckingham and J.A. Pople, *Proc. Phys. Soc.*, **68A**, 905 (1955).

9. A.D. Buckingham and J.A. Pople, *Proc. Phys. Soc.*, **69B**, 1133 (1956).

10. A.D. Buckingham, *Advan. Chem. Phys.*, **12**, 107 (1967).

11. A.D. Buckingham and M.J. Jamieson, *Molec. Phys.*, **22**, 117 (1971).

12. A.D. Buckingham and M. Pariseau, *Trans. Faraday Soc.*, **62**, 1 (1966).

13. A.D. Buckingham, R.L. Disch and D.A. Dunmur, *J. Am. Chem. Soc.*, **90**, 3104 (1968).

14. A.D. Buckingham, C. Graham and J.H. Williams, *Molec. Phys.*, **49**, 703 (1983).

15. C. Graham, J. Pierrus and R.E. Raab, *Molec. Phys.*, **67**, 939 (1989).

16. D.A. Imrie and R.E. Raab, *Molec. Phys.*, **74**, 833 (1991).

17. I.R. Gentle, D.R. Laver and G.L.D. Ritchie, *J. Phys. Chem.*, **93**, 3035 (1989).

18. I.R. Gentle and G.L.D. Ritchie, *J. Phys. Chem.*, **93**, 7740 (1989).

19. I.R. Gentle and G.L.D. Ritchie, *J. Phys. Chem.*, **94**, 1844 (1990).

20. P.B. Lukins, A.D. Buckingham and G.L.D. Ritchie, *J. Phys. Chem.*, **88**, 2414 (1984)

21. I.E. Craven, M.R. Hesling, D.R. Laver, P.B. Lukins, G.L.D. Ritchie and J. Vrbancich, *J. Phys. Chem.*, **93**, 627 (1989).

22. M.H. Coonan and G.L.D. Ritchie, *Chem. Phys. Lett.*, **202**, 237 (1993).

23. Krishnaji and V. Prakash, *Rev. Mod. Phys.*, **38**, 690 (1966).

24. J.A. Pople, *Proc. Roy. Soc.(London)*, **A221**, 498 (1954).

25. R.H. Orcutt, *J. Chem. Phys.*, **39**, 605 (1963).

26. S. Kielich, *Physica*, **28**, 511 (1962).

27. A.D. Buckingham and J.A. Pople, *Trans. Faraday Soc.*, **51**, 1029 (1955).

28. T.K. Bose and R.H. Cole, *J. Chem. Phys.*, **52**, 140 (1970).

29. J Huot and T.K. Bose, *J. Chem. Phys.*, **94**, 3849 (1991).

30. J.D. Poll and J. Van Kranendonk, *Can. J. Phys.*, **39**, 189 (1961).

31. W. Ho, G. Birnbaum and A. Rosenberg, *J. Chem. Phys.*, **55**, 1028 (1971).

32. A. Rastogi and R.P. Lowndes, *J. Phys. B*, **10**, 495 (1977).

33. I.R. Dagg, W. Smith and L.A.A. Read, *Can. J. Phys.*,**60**, 16 (1982).

34. W. Hüttner and W.H. Flygare, *J. Chem. Phys.*, **47**, 4137 (1967).

35. W.H. Flygare and R.C. Benson, *Molec. Phys.*, **20**, 225 (1971).

36. S.L. Hartford, W.C. Allen, C.L. Norris, E.F. Pearson and W.H. Flygare, *Chem. Phys. Lett.*, **18**, 153 (!973).

37. W.H. Flygare, *Chem. Rev.*, **74**, 653 (1974).

38. F.E. Budenholzer, E.A. Gislason, A.D. Jorgensen and J.G. Sachs, *Chem. Phys. Lett.*, **47**, 429 (1977).

39. M. Bloom, I. Oppenheim, M. Lipsicas, C.G. Wade and C.F. Yarnell, *J. Chem. Phys.*, **43**, 1036 (1965).

40. G. Maroulis and A.J. Thakkar, *J. Chem. Phys.*, **93**, 4164 (1990).

41. I. Cerusak, G.H.F. Diercksen and A.J. Sadlej, *Chem. Phys.*, **108**, 45 (1986).

42. R. Lindh and B. Liu, *J. Chem. Phys.*, **94**, 4356 (1990).

43. R.J. Emrich and W. Steele, *Molec. Phys.*, **40**, 469 (1980).

44. M.R. Battaglia, A.D. Buckingham and J.H. Williams, *Chem. Phys. Lett.*, **78**, 421 (1981).

45. M.R. Battaglia, A.D. Buckingham, D. Neumark, R.K. Pierens and J.H. Williams, *Molec. Phys.*, **43**, 1015 (1981).

46. J. Vrbancich and G.L.D. Ritchie, *J. Chem. Soc. Faraday II*, **76**, 648 (1980).

47. J. Vrbancich and G.L.D. Ritchie, *J. Chem. Soc. Faraday II*, **76**, 1245 (1980).

48. J. Vrbancich and G.L.D. Ritchie, *Chem. Phys. Lett.*, **94**, 63 (1982).

49. G.R. Dennis and G.L.D. Ritchie, *J. Phys. Chem.*, **95**, 656 (1991).

CHAPTER 2 - PRINCIPLES OF THE FIELD GRADIENT BIREFRINGENCE APPARATUS

2.1 INTRODUCTION

The basic principles involved in the development of equipment to measure the temperature dependence of the field gradient induced birefringence effect of gases and vapours are presented and discussed in this chapter.

In general, the aim of the experiment is to measure the molar field gradient birefringence constant, ${}_{\mathrm{m}}Q$, of a gas as a function of temperature. The expression for ${}_{\mathrm{m}}Q$ is

$$ {}_{\mathrm{m}}Q = \frac{2V_{\mathrm{m}}}{3}\left[\frac{n_x - n_y}{E_{xx}}\right] \tag{2.1} $$

Hence, in order to evaluate ${}_{\mathrm{m}}Q$ it is necessary to determine $n_x - n_y$, E_{xx}, V_{m} and T.

Instead of measuring the birefringence directly, the experiment is designed to measure the phase retardation, induced by the applied field gradient, of the elliptically polarized emergent laser beam. When the beam emerges from the gas quadrupole cell, the degree of ellipticity is characterized by a phase angle, δ, called the retardance. This quantity is related to the birefringence by

$$ \delta = \frac{2\pi l}{\lambda}\left(n_x - n_y\right) \tag{2.2} $$

where λ is the vacuum wavelength of the light and l is the pathlength in the medium.

The largest source of uncertainty in this experiment arises from the measurement of δ. Due to the relatively small magnitude of δ (typically $< 10^{-7}$ rad), when compared to other optical experiments such as the electrooptical Kerr effect ($\delta > 10^{-6}$ rad), very precise techniques are necessary to measure this quantity. One convenient and sensitive method is to use a calibrated retarder to apply a nulling retardance. A Faraday coil and Kerr cell are two examples of commonly used calibrated retarders. In order to increase the size of the induced birefringence, several modifications of the apparatus were considered. These included: 1) a longer optical pathlength; 2) the use of a He-Cd laser; and 3) applying a larger electric field gradient. For various reasons, which will be mentioned in the following chapters, these modifications are limited in their applications.

To determine the most effective method for measuring the field induced retardance, several techniques employed by other workers [1-3] were considered. All of these techniques use the linear method of detection developed by Badoz.[4] This involves adding a separate birefringence element to the induced field gradient birefringence. If this additional birefringence is placed in the elliptically polarized light beam, such that the axes of its polarization ellipsoid are parallel to those of the gas quadrupole cell, then the total retardance will be the sum of the values of δ for the two elements. If δ_1 is the retardance induced by the electric field gradient modulated at a specific frequency, and δ_2 is the additional static retardance, the alternating component of the light intensity passing the analyzer is given by [2]

$$I = \frac{1}{4} I_0 \left({\delta_1}^2 + 2\delta_1\delta_2 \right) \tag{2.3}$$

As the first term involving ${\delta_1}^2$ is vanishingly small, detection of δ_1, which has been made several orders of magnitude larger by δ_2, is effected by tuning to the fundamental frequency.

The following nulling arrangements have been used by previous workers:

1) a Kerr cell, containing two pairs of electrodes, where one set provides the modulated nulling signal and the other set a static retardance;[1]

2) a Kerr cell, with one set of electrodes to provide the nulling signal and an offset in the quarterwave plate to produce the static retardance;[2] and

3) a Faraday coil to null the induced retardance and an offset in the quarterwave plate to produce the static retardance.[3]

Having considered these procedures and several others, it was decided the arrangement consisting of the Faraday coil and an offset in the alignment of the quarterwave plate was the most efficient for this experiment. This method involves offsetting the quarterwave plate by a small angle, $\varepsilon < 1°$, so that the azimuth of the quarterwave plate is then $45° + \varepsilon$. The signal arising from the birefringence induced in the quadrupole cell, as monitored by the lock-in amplifier, is then nulled from one end of the scale on the lock-in amplifier to the other by increasing the current through the Faraday coil. This provides a straight-line plot of lock-in amplifier output against Faraday coil current. The process is then repeated with the quarterwave plate offset in the opposite direction (azimuth $45° - \varepsilon$). The results are then plotted on a graph, as shown in Figure 2.1, where the intersection of the two lines, corresponding to $\pm \varepsilon$, determines the true null point. This procedure is discussed further in Section 2.3 and, in particular, how it excludes any spurious birefringence introduced by the windows of the quadrupole cell.

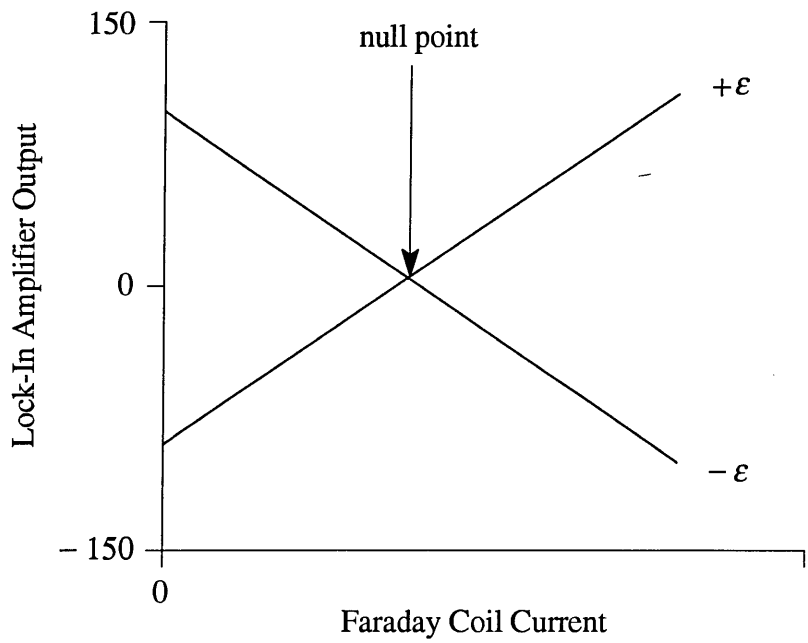

Figure 2.1 Procedure used to determine the null point.

2.2 PRINCIPLES OF THE FIELD GRADIENT BIREFRINGENCE EXPERIMENT

The basic optical components for the field gradient birefringence experiment are similar to those used by other workers,[3] and are shown schematically in Figure 2.2. The laboratory axis system is chosen in which the + z-axis is in the direction of propagation of the beam, the + x-axis is perpendicular to the plane of the wires in the gas quadrupole cell (vertical), and the + y-axis is orthogonal to the x and z axes. For each component, the azimuth is defined relative to the x-axis.

Light from a plane-polarized He-Ne laser traverses a polarizing prism with its transmission axis orientated at $\pi/4$ with respect to the plane of the wires, and the ellipticity induced in the beam by the birefringent gas is converted to a rotation by a

quarterwave plate, and is then nulled using a Faraday coil. Light passing the analyzer is detected by the photodiode. The intensity of light reaching the photodiode contains contributions modulated at frequencies of ω and 2ω. Using bandpass filters and a lock-in amplifier tuned to the fundamental, the signal from the Kerr effect can be eliminated.

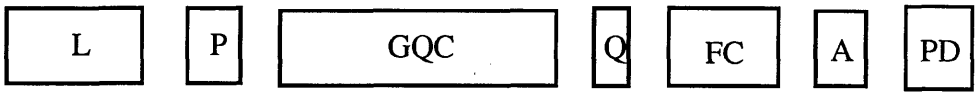

Figure 2.2 Optical configuration of the field gradient birefringence apparatus. L, laser; P, polarizer; GQC, gas quadrupole cell; Q, quarterwave plate; FC, Faraday coil; A, analyzer; PD, photodiode.

The relative retardance δ_g introduced in the gas quadrupole cell may be expressed as [5]

$$\delta_g = kV_0 \sin \omega t + k_1 V_0^2 \sin^2 \omega t \qquad (2.4)$$

where $V_0 \sin \omega t$ is the applied potential and k, k_1 are constants which depend on the geometry of the gas quadrupole cell and on the substance within the cell. Along the axis of the cell, k_1 may be zero, but generally this is not the case. The calibrated nulling rotation provided by the Faraday coil is

$$\theta' = \theta^0 \sin(\omega t + \phi) \qquad (2.5)$$

where ω is the angular frequency of the current through the Faraday coil, θ^0 is the peak amplitude and ϕ is the phase.

2.3 JONES CALCULUS

In order to determine the intensity of light reaching the detector, Jones calculus is applied to the optical sequence shown in Figure 2.3. The derivation of the necessary matrices together with discussions on their applications have been provided by other authors, and only the relevant results are presented here.[3,6]

The Jones vector for the electric field associated with a plane-polarized light beam is given by [6]

$$\upsilon = E_0 \begin{vmatrix} \cos(\alpha)\exp(i\beta/2) \\ \sin(\alpha)\exp(-i\beta/2) \end{vmatrix} \tag{2.6}$$

where $E_0 = \left(E_x^2 + E_y^2\right)^{\frac{1}{2}} \exp\left[i\left(\beta_x + \beta_y\right)/2\right]$ and $\alpha = \tan^{-1}\left(E_y/E_x\right)$.

Optical components that conserve the intensity of the light beam can be described using the following unitary matrices:[6]

1) a linear retarder

$$J(\delta,\theta) = \begin{vmatrix} e^{i\beta/2}\cos^2(\theta) + e^{-i\beta/2}\sin^2(\theta) & \left(e^{i\beta/2} - e^{-i\beta/2}\right)\sin(\theta)\cos(\theta) \\ \left(e^{i\beta/2} - e^{-i\beta/2}\right)\sin(\theta)\cos(\theta) & e^{i\beta/2}\sin^2(\theta) + e^{-i\beta/2}\cos^2(\theta) \end{vmatrix} \tag{2.7}$$

where δ is the optical retardance and θ is the azimuth;

2) a left-circular rotator

$$R(\theta) = \begin{vmatrix} \cos(\theta) & \sin(\theta) \\ -\sin(\theta) & \cos(\theta) \end{vmatrix} \tag{2.8}$$

where θ is the Faraday rotation; and

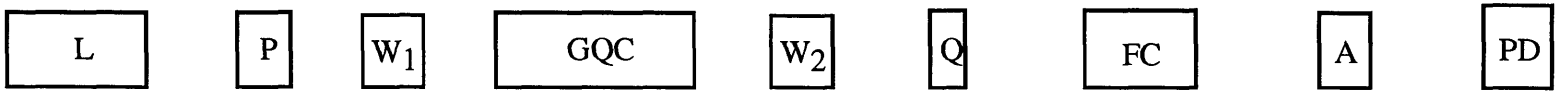

Azimuth		$\frac{\pi}{4}$	θ_1	0	θ_2	$\frac{\pi}{4} \pm \varepsilon$		$-\frac{\pi}{4} + \alpha$
Retardance		0	β_1	δ	β_2	$\frac{\pi}{2}$		0
Rotation							θ	
Jones vector		P	S_1	J_1	S_2	J_2	R	P

Figure 2.3 The optical system used in the Jones calculus analysis. Each component is specified in terms of its optical properties and corresponding Jones vector. The entrance and exit window of the quadrupole cell are represented by W_1 and W_2, respectively.

3) a polarizer

$$P(\theta) = \begin{vmatrix} \cos^2(\theta) & \sin(\theta)\cos(\theta) \\ \sin(\theta)\cos(\theta) & \sin^2(\theta) \end{vmatrix} \tag{2.9}$$

where θ is the azimuth of the transmission axis.

Thus, for the optical system shown in Figure 2.3, which includes the two windows of the quadrupole cell, with retardances β_1 and β_2 in the entrance and exit windows at corresponding azimuths, θ_1 and θ_2, the normalized Jones vector υ describing the polarized monochromatic light wave leaving the analyzer is [3]

$$\upsilon = P\left(-\frac{\pi}{4}+\alpha\right)R(\theta)J_2\left(\frac{\pi}{2},\frac{\pi}{4}\pm\varepsilon\right)S_2(\beta_2,\theta_2)J_1(\delta,0)S_1(\beta_1,\theta_1)\upsilon_0 \tag{2.10}$$

where υ_0 is the normalized Jones vector describing the light wave leaving the polarizer and S, J, P denote Jones matrices for the following components: S_1 and S_2 are for the entrance and exit windows, respectively, of the quadrupole cell; $J_1$and J_2 are for the quadrupole cell and quarterwave plate; and P is the analyzer.

A considerable simplification of this calculation can be made by expressing J and R as linear combinations of Pauli matrices and of the unit matrix such that [6]

$$J(\delta,\theta) = \cos(\delta/2)\,\mathrm{I}+\sin(\delta/2)\cos(2\theta)\,\mathrm{i}+\sin(\delta/2)\sin(2\theta)\,\mathrm{k}$$

$$R(\theta) = \cos(\theta)\,\mathrm{I}-\sin(\theta)\,\mathrm{j}$$

and by expressing P as $P(\alpha)\upsilon_\beta = \cos(\alpha-\beta)\upsilon_\alpha$, where $\upsilon_\alpha = \begin{vmatrix} \cos(\alpha) \\ \sin(\alpha) \end{vmatrix}$. [3]

The expression for the total intensity of the light beam reaching the photodiode is given by [3]

$$I = \upsilon\upsilon^* I_0 \tag{2.11}$$

where I_0 is the intensity of the beam leaving the polarizer. Of the total intensity I, only the modulated component, at a frequency of ω, is of interest. Using a small angle expansion to extract the modulated contribution to the intensity, the following expression is obtained [3]

$$I_\omega = I_0\left\{2(\alpha + C_1 + C_2 \pm \varepsilon)\theta + \left[\alpha + C_1 + C_2 \pm \varepsilon(1 - 2S_2)\right]\delta\right\} \tag{2.12}$$

in which $C_n = \frac{1}{2}\beta_n \cos 2\theta_n$, $S_n = \frac{1}{2}\beta_n \sin 2\theta_n$ and $n = 1, 2$.

From a plot of I vs θ, the intersection of the two lines corresponding to $\pm\,\varepsilon$ yields the null position. If the effects of window birefringence are ignored, such that $C_n = S_n = 0$, then equation (2.12) reduces to [3]

$$I_\omega = I_0\left\{(\alpha \pm \varepsilon)(2\theta + \delta)\right\} \tag{2.13}$$

In this case, the null position occurs at $\theta = -\frac{1}{2}\delta$, which corresponds to $I_\omega = 0$ and zero output on the lock-in amplifier.

However, if window birefringence exists, the point of intersection occurs at

$$\theta = -\frac{1}{2}(1 - 2S_2)\delta \tag{2.14}$$

Substituting $\theta = -\frac{1}{2}(1-2S_2)\delta$ into equation (2.12), the intensity at the point of intersection is found to be [3]

$$I_\omega = 2I_0S_2(\alpha + C_1 + C_2)\delta \qquad (2.15)$$

which is obviously not zero. Thus, in the presence of window birefringence, the null position does not occur at zero output on the lock-in amplifier.

As the detection system used in this experiment does not have a reference baseline to aid in the extraction of δ, this intersection of lines method is used to obtain the nulling current, thus eliminating any stray birefringence introduced by the cell windows.

The retardance of the quarterwave plate is another possible source of error that needs to be considered. When the apparatus was first assembled, a dual-wavelength quarterwave plate (488.0 nm and 632.8 nm) was used in the optical system. The reason for using the dual-wavelength quarterwave plate came from the possibility that measurements may be performed at a shorter wavelength, thereby increasing the size of the induced birefringence. However, when the initial results for carbon dioxide were obtained, the values seemed to be too high when compared to previous results, hence an investigation of possible sources of error was conducted. When the quarterwave plate was rotated through 90°, it was found that the results decreased by ≈ 20%. A new zero-order quarterwave plate was ordered, and initial tests showed that the results for all orientations, about the fast and slow axes, produced values that were within 1% of each other. Consequently, any possible error arising from the retardance of the quarterwave plate has been eliminated.

Any errors due to the misalignment of the optical components are considered negligible in this experiment. Using measurements of ${}_{m}Q$ for carbon dioxide at room temperature as a reference, the apparatus can be dismantled and reassembled to give results within 1% of the standard.

2.4 CALCULATION OF THE ELECTRIC FIELD GRADIENT

The electrode design, used to establish a known field gradient, is based on a two-wire arrangement similar to that previously used by other workers.[1-3] The quadrupole cell consists of two fine taut parallel wires of radius r, separated by a distance $2d$ (taken from the centre of each wire), and located such that a line midway between them is at the centre of an earthed conducting cylinder having radius a. For a typical design $(d/r) \approx (a/d) \approx 10$. Buckingham and Disch [1] outlined the procedure for calculating the electric field gradient based on the geometry of the cell. A cross-sectional view, together with relevant parameters, is shown in Figure 2.4.

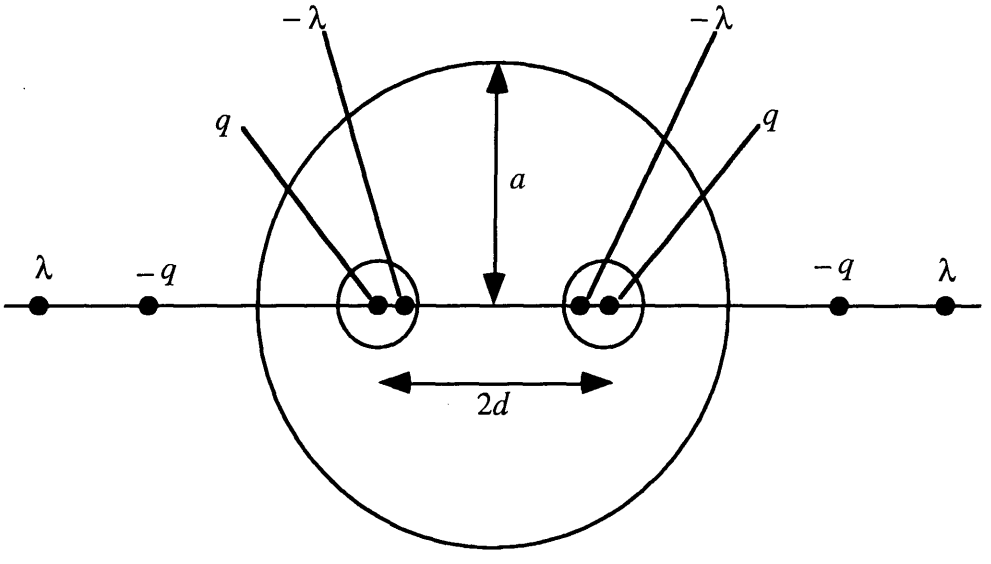

Figure 2.4 Cross sectional view of the two-wire cell (not drawn to scale) with the four pairs of line charges used to calculate the magnitude of the field gradient.

Buckingham and Disch solved the problem in two dimensions, by attributing the electric field gradient between the two wires to two line charges of q located on the axes of the two wires. As the diameter of the wires is not negligible with respect to their separation, the surfaces of the wires will not coincide with equipotential surfaces, so two image line charges, λ, are placed within the wire boundaries at inverse points with respect to each other. Similarly, the inner surface of the earthed cylinder is not an equipotential surface, so two more pairs of image line charges are placed outside the boundary of the cylinder. Hence, to calculate accurately the magnitude of the field gradient, a knowledge of the size and position of the image charges used to represent the wires and inner surface of the cell is required. These are calculated using the following relations:[5]

$$\begin{aligned} q &= (4\pi\varepsilon_0 V_0)/\ln(a^2/2rd) \\ \lambda &= (q/2)\left[r^2(2d-b)/d(2bd-b^2+r^2)\right] \\ b &= \left[r^2(4d^2-r^2)/4d(2d^2+r^2)\right] \\ t' &= a^2/(d-b) \\ t &= a^2/d \end{aligned} \tag{2.16}$$

where b is the distance between the central line charge of q and the image line charge of $-\lambda$ within the same wire boundary.

Thus, from the above equations, the average value of the electric field gradient E_{xx} over the circular region of the light beam about the cell axis is [5]

$$E_{xx} = (\pi\varepsilon_0)^{-1}\left[-\frac{q}{d^2} + \frac{q}{t^2} + \frac{\lambda}{(d-b)^2} - \frac{\lambda}{t'^2}\right] \tag{2.17}$$

In this section, the main principles of the experimental method have been discussed with particular emphasis given to the measurement of δ and the calculation of E_{xx}. These two quantities provide the most significant sources of error in calculating ${}_{m}Q$, as T and p are easily measured. In the case of determining δ, several optical errors that are important when assessing the reliability of the results obtained using this apparatus, have been briefly addressed. Several other potential sources of error, including calibration errors, are discussed in the relevant sections of the following chapter.

2.5 REFERENCES

1. A.D. Buckingham and R.L. Disch, *Proc. R. Soc. A*, **273**, 275 (1963).

2. M.R. Battaglia, A.D. Buckingham, D. Neumark, R.K. Pierens and J.H. Williams, *Molec. Phys.*, **43**, 1015 (1981).

3. C. Graham, J. Pierrus and R.E. Raab, *Molec. Phys.*, **67**, 939 (1989).

4. J. Badoz, *J. Physique Radium*, **17**, 143A (1956).

5. J. Vrbancich, M.P. Bogaard and G.L.D. Ritchie, *J. Phys. E: Sci. Instrum.*, **14**, 166 (1981).

6. R. Piazza, V. Degiorgio, T. Bellini, *Optics Commun.*, **58**, 400 (1986).

CHAPTER 3 – APPARATUS FOR THE MEASUREMENT OF FIELD GRADIENT INDUCED BIREFRINGENCE IN GASES

3.1 INTRODUCTION

The apparatus for the measurement of field gradient induced birefringence in gases, designed and constructed at the University of New England, is described in this chapter. An outline of the technique used in the measurements is also given. A schematic diagram of the apparatus is shown in Figure 3.1.

3.2 FRAMEWORK

The main requirements considered when designing the optical bench were that it had to be mechanically stable and, in addition, be capable of isolating any vibrations to the optical components from the surroundings that may have contributed to the noise in the experiment. The bench was constructed from four rectangular cement pillars, 860 mm high, resting on antivibration pads, supporting a flat cement slab of dimensions $4000 \times 660 \times 130$ mm. Antivibration padding was also placed between the pillars and the slab. The optical rail, made from H-section steel, is bolted to the cement slab and supported by four steel mounts that have rubber pads on their feet, further reducing any vibrational interference.

All the optical components are mounted on steel stands that provide a stable base and through simple mechanisms allow fine adjustments in all directions.

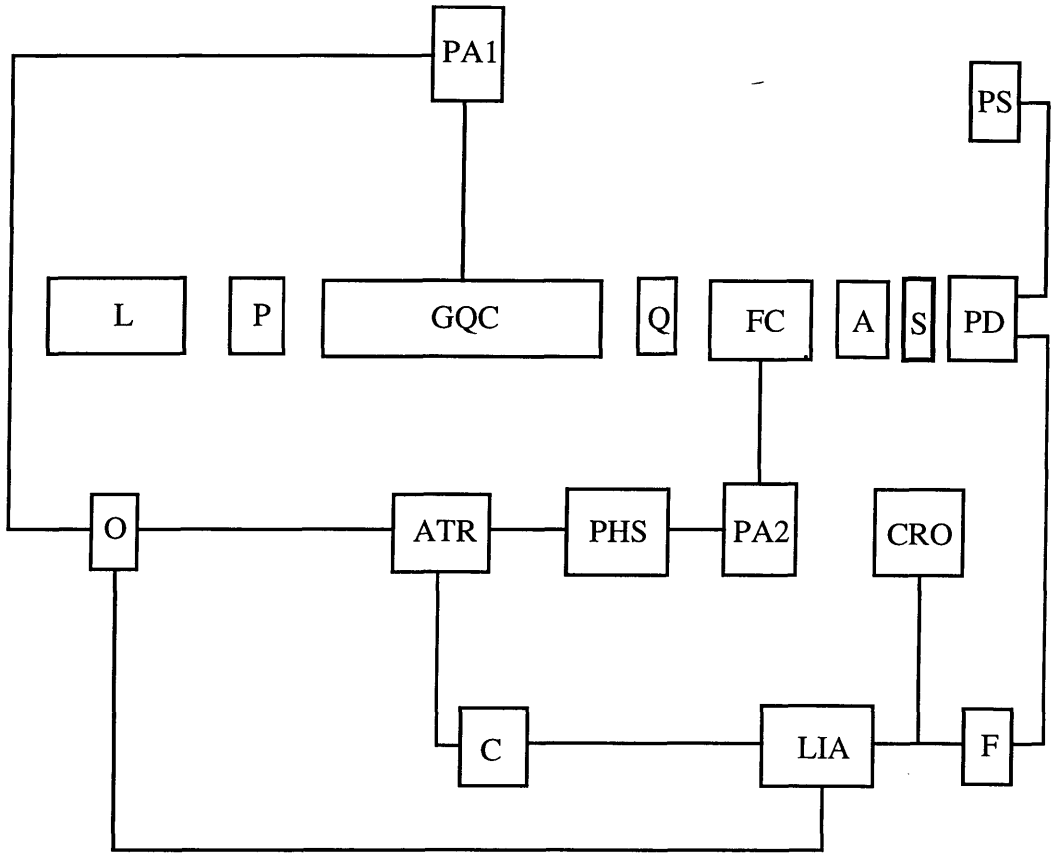

Figure 3.1 Apparatus for the measurement of field gradient induced birefringence. L, laser; P, polarizer; GQC, gas quadrupole cell; PA1, power amplifier for quadrupole cell; Q, quarterwave plate; FC, Faraday coil; A, analyzer; S, stop; PD, photodiode; PS, photodiode power supply; CRO, oscilloscope; F, filter; LIA, lock-in amplifier; PA2, power amplifier for Faraday coil; PHS, phase shifter; ATR, attenuator; O, oscillator; C, computer.

3.3 LASER AND OPTICS

A plane-polarized He-Ne laser (Uniphase Model 1335P) was used for all the measurements performed in the present study. This laser is rated at 10 mW TEM_{00} at 632.8 nm and has a minimum polarization ratio of 500:1. The beam diameter at $1/e^2$ points is 0.68 ± 0.02 mm with a beam divergence of 1.2 mrad. Laser noise is 1% rms (30 Hz – 10 MHz).

The polarizer and analyzer are both Glan-Taylor prisms (Karl Lambrecht Corporation) with 8 mm clear apertures. They have an extinction ratio of 5×10^{-6} at 2/3 or less of full aperture. They are each mounted in a precision rotator (Oriel Corporation Model 13011) where a fine micrometer adjustment enables a high resolution setting to within 0.1 s.

A zero-order quartz quarterwave plate (Newport Model 05RP04), mounted in a rotator similar to those described above, was used for all the measurements performed in this study. This quarterwave plate was chosen for two reasons. Firstly, the retardance of the plate was found to be 90° ± 1%. Secondly, because measurements were performed over a range of temperatures, the quarterwave plate would have experienced temperature changes due to its location near the oven surrounding the gas quadrupole cell. If a single- or dual-wavelength quarterwave plate had been used, errors may have arisen due to changes in the retardance of the quarterwave plate with temperature shifts. However, zero-order quarterwave plates are temperature insensitive phase retarders and this problem is eliminated.

An aluminium plate with a 1 mm diameter hole drilled through its centre, was inserted between the analyzer and photodiode, thus preventing any spuriously scattered light or back reflections of the laser beam from reaching the photodiode.

3.4 THE GAS QUADRUPOLE CELL

The gas quadrupole cell was designed so that it could satisfy the following conditions: 1) withstand a pressure range from vacuum to ≈ 3500 kPa; 2) withstand a temperature range from room temperature to 500 K; 3) withstand a high potential without discharging.

The quadrupole cell described here satisfies all the above conditions, although for various reasons which will be discussed below, measurements were not performed at the upper limits of these ranges.

A diagram of the cell is shown in Figure 3.2. The cell is constructed from a 2010 mm length of stainless steel tube of 54.6 mm inside diameter and 3 mm wall thickness, with stainless steel flanges welded to each end of the tube. Stainless steel end-caps support stainless steel tubes on which the window housings are mounted. Sealing between the flanges and end-caps is effected by Viton O-rings. The window housings are brass cylinders with a cavity in which the windows are lightly held between Viton O-rings. The cell windows are made from Schott SF 57 optical glass of 10 mm diameter and 8 mm thickness. With the housings mounted on steel tubes extending 70 mm from the cell, retardation in the windows induced by the applied electric field gradient is negligible.

The cell has three opposing pairs of viewing ports spaced along its length. These ports are very similar in construction to the window housings described earlier. The windows for the ports are made from fused silica and are mounted at the end of 50 mm lengths of stainless steel tube which, in turn, are welded into holes bored along the length of the cell. The viewing ports enable the wire separation to be accurately determined using a travelling microscope in conjunction with a digital measuring system (Bausch and Lomb Model AR II). This system has a resolution of 5 μm.

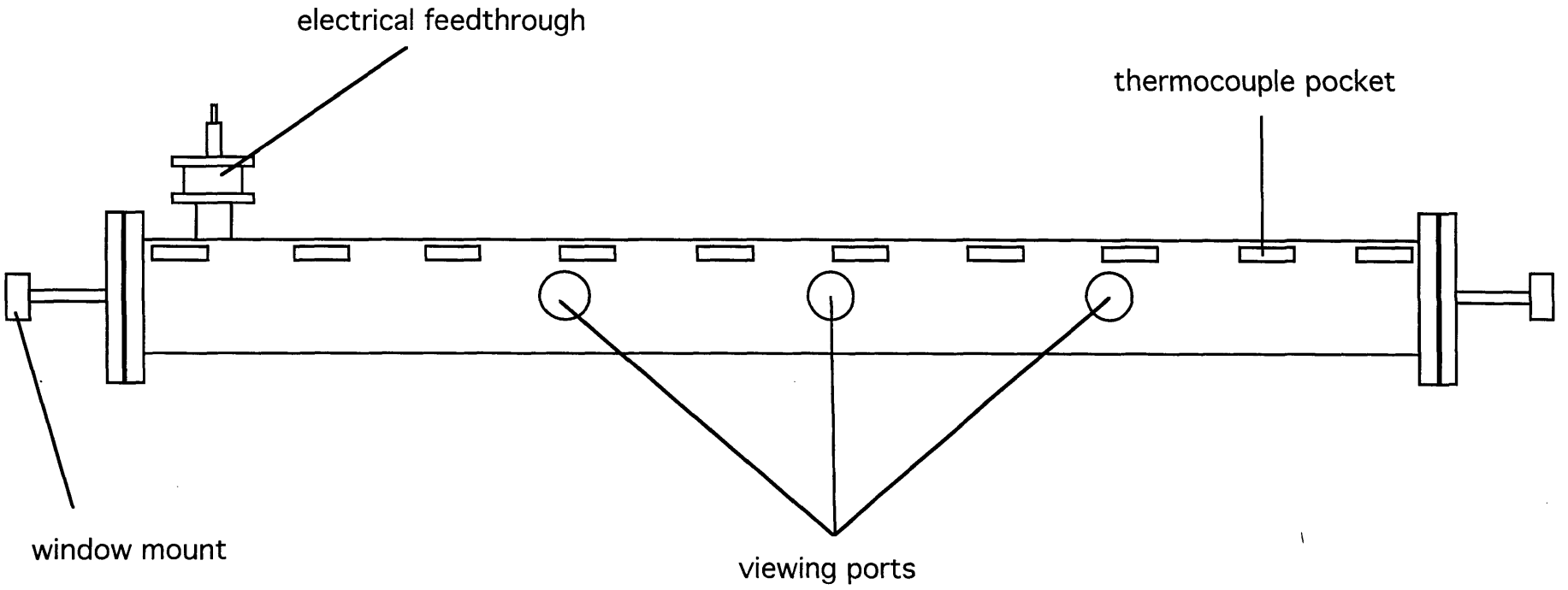

Figure 3.2 The quadrupole cell.

Inside the cell, as shown in Figure 3.3, are the two wire-holders that provide the tension in the wires. At one end there are two small tensioning mechanisms on to which the wire is wound, and they allow the wire to be set to the required tension. A stainless-steel spring loaded device located at the other end maintains the tension in the wires. Located on the front of each wire holder is a plate that has three accurately positioned holes, which ensure that the wires are separated at a fixed predetermined distance and that the laser beam passes along the axis between them. Other holes in the plate allow a free flow of the gas when filling and evacuating the cell. The mountings for the wire holders are made from Macor ceramic glass. This material was chosen because of its special qualities which include: 1) it has a maximum operating temperature of 1300 K; 2) it is an excellent insulator at high voltages; 3) it is resistant to most chemicals; 4) it is mechanically stable.

The electrical feedthrough consists of a stainless steel rod with threads at both ends, running through the centre of a glass ceramic cylinder. A small length of stainless steel wire fastened to the end of the feedthrough inside the cell completes the connection to the wire-holder, as shown by Figure 3.4. This set-up proved quite satisfactory with little risk of corona discharges under the operating conditions.

3.5 POWER SUPPLIES

A signal generator (Goodwill, Model GFG-8015G), operating at 389 Hz, provides the sinusoidal reference voltage for the experiment. The high voltage applied to the quadrupole cell is provided by a power amplifier / transformer arrangement. A commercial 100 W audio power amplifier drives a 150:1 step-up high voltage transformer. This arrangement proved more than adequate in supplying the operating voltages in the range 1.0 – 3.5 kV used for the measurements performed in this project.

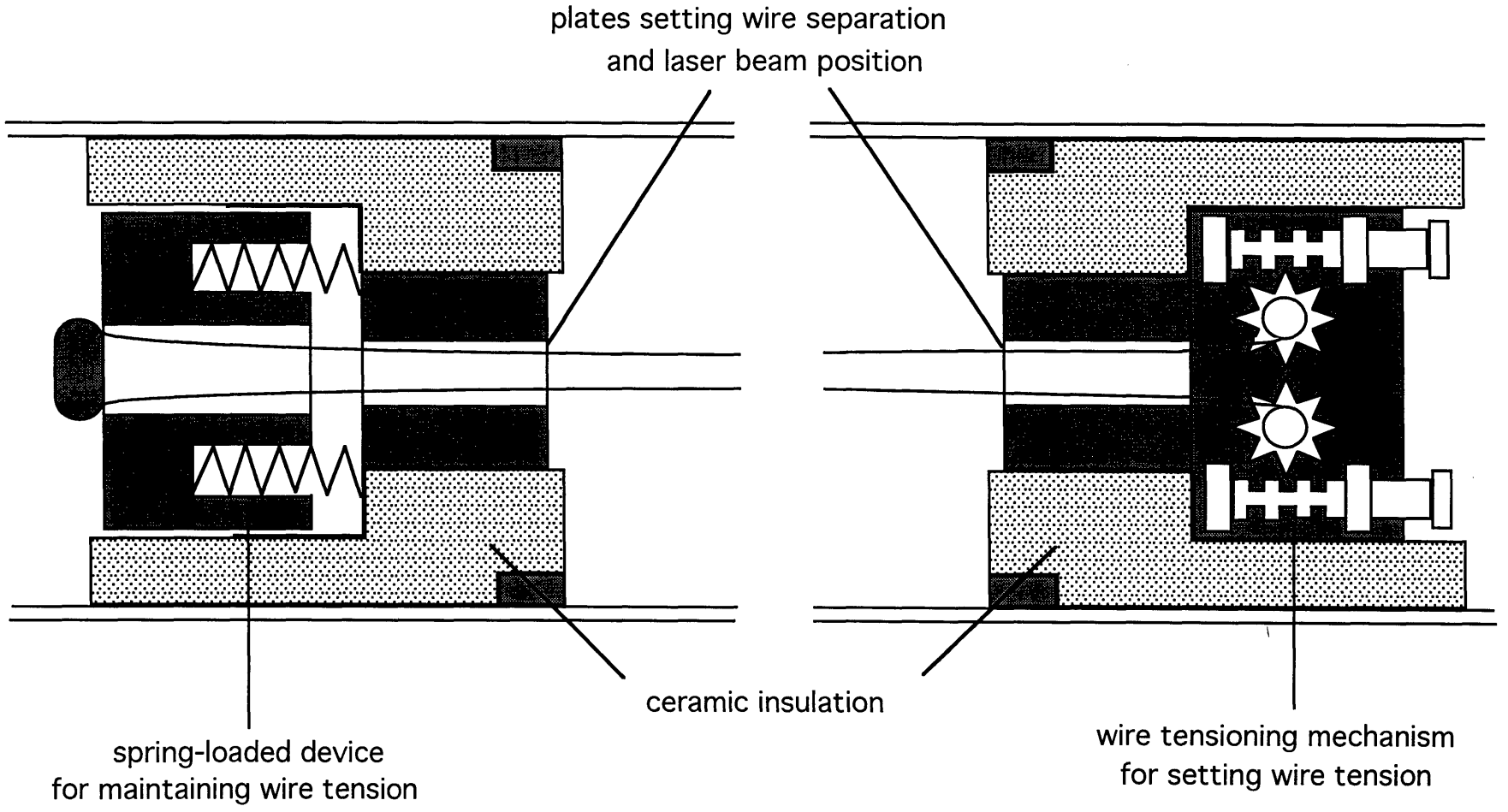

Figure 3.3 Cross section of the wire holders used to establish and maintain the wire tension.

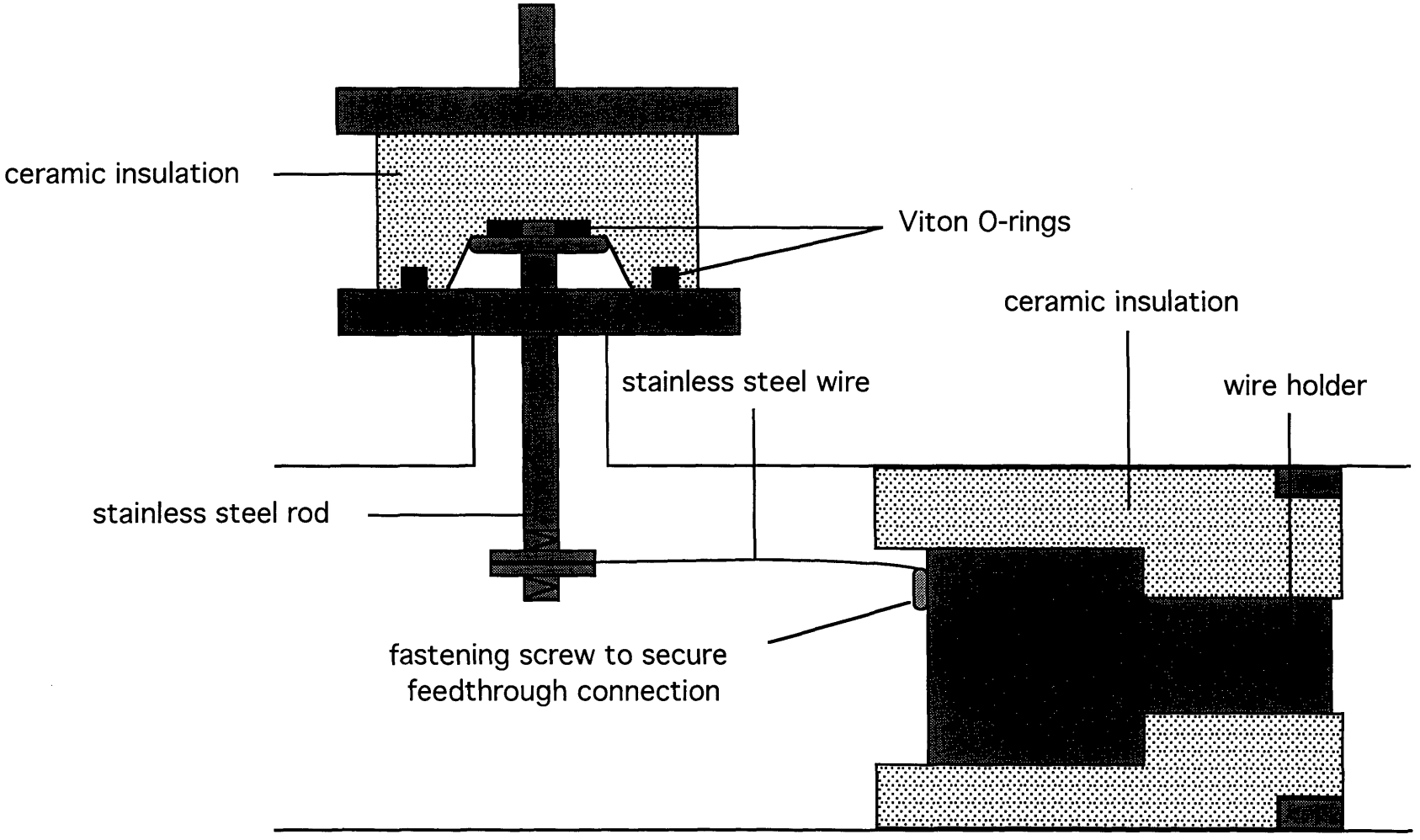

Figure 3.4 Connection between the electrical feedthrough and the wire holder.

The voltage applied to the quadrupole cell depended on the density and the breakdown potential of the gas in the cell. It was measured using a high voltage probe (Fluke Model 80K-6) in conjunction with a digital voltmeter (Fluke Model 45, 0.2% accuracy) providing an accuracy of ± 1%. No distortion of the output voltage waveform from this arrangement was observed.

A commercial 20 W audio power amplifier is used to provide the stable current for the Faraday coil. This is discussed further in section 3.9.

3.6 FARADAY COIL

The primary function of the Faraday coil is to provide a nulling signal at a frequency of ω; however, it also serves in the alignment of the analyzer and quarterwave plate. The coil consists of a 155 mm perspex tube of 25 mm diameter with 150 turns of 19-gauge transformer wire. Housings for the windows (polished fused quartz 1 mm thick, 10 mm diameter) are constructed from threaded brass mounts, Viton O-rings and screw-on caps that also act as dust covers.

Distilled water, passed through a 0.15 μm millipore filter, fills the coil cavity. Water, which has a large Verdet constant, was found to be very convenient.

Section 3.14 describes the procedures used to calibrate the Faraday coil.

3.7 THE OVEN FOR THE QUADRUPOLE CELL

Version 1

Initially, the heating of the quadrupole cell was achieved as follows: grounded electrical heating tape (KPG-75 W m^{-1}) was wrapped directly around the cell body. This

was followed by a layer of Refrasil insulation tape. A sheet metal shell, lined with a 50 mm layer of ceramic fibre wool, then encased the cell body. The window mounts were independently wrapped with heating tape and insulated with fibreglass tape. A West Opus temperature controller using a J-type thermocouple sensor controlled the temperature of the cell. The temperature of the cell windows was controlled by a Variac autotransformer.

This method of heating proved inadequate, however, due to temperature inhomogeneity along the length of the cell. The non-uniform temperature was produced by a combination of unevenness in the heater winding and insulation around the cell, and resulted in bending of the laser beam when working with pressures above 250 kPa. The spatial non-uniformities in gas density caused the intensity of the beam to fluctuate severely on emerging from the cell, thus making any measurements unreliable. Many attempts were made to eliminate these temperature gradients by adjusting the heating tape and/or the insulation, but all proved unsuccessful. A new oven was then designed and constructed.

Version 2

Instead of directly heating the cell with heating tape, an air oven that encased the whole cell, including the windows, was constructed. A large tube, 270 mm diameter and 2400 mm in length fabricated from sheet metal 1.5 mm thick, provided an internal shell for the oven. Heating tape (KPG-75 W m^{-1}) was wrapped around the outside of the tube, which was then covered by a large Refrasil blanket. Heatlock pipe insulation 50 mm thick provided the lagging. End-caps thermally insulated with fibreglass matting 60 mm thick completed the oven. A West Opus temperature controller, capable of maintaining a constant temperature to $\pm$ 0.2 K, supplied the power to the heating tape. With the large internal volume of the oven, any temperature gradients were suppressed

due to the natural convection of the air. A cross-section of the oven is shown in Figure 3.5.

The temperature inside the oven and consequently the quadrupole cell is monitored by a series of 10 K-type thermocouples located in small pockets evenly placed along the length of the cell (as shown in Figure 3.2). A Digitron Model 3900 KTJ panel meter with a 12-way selector switch displays the temperature of each thermocouple. The accuracy of temperatures measured using this method is better than ± 1 K.

Small hollow tubes (diameter 8 mm), centrally fitted in the end caps, allow the laser beam to enter, pass through the quadrupole cell and emerge from the oven unperturbed. In addition, a stainless-steel tube connecting the gas handling system to the cell, passes through a hole in the front end cap. Also, holes strategically positioned in the oven wall enable easy access to the viewing ports and the electrical feedthrough.

3.8 LIGHT DETECTOR

When the apparatus was first assembled, a photomultiplier was used to detect the intensity of the transmitted light. However, with the offset of the quarterwave plate to amplify the signal, the shot noise of the photomultiplier also increased significantly. It was found that, when measuring relatively small effects, it became very difficult to separate the signal from the noise. Hence an investigation into using a silicon photodiode was conducted.

The shot-noise limit (SNL) to the sensitivity of a measurement is given by [1]

$$\phi_{SNL} = \left(F_0 Q \Delta T\right)^{-1/2} \tag{3.1}$$

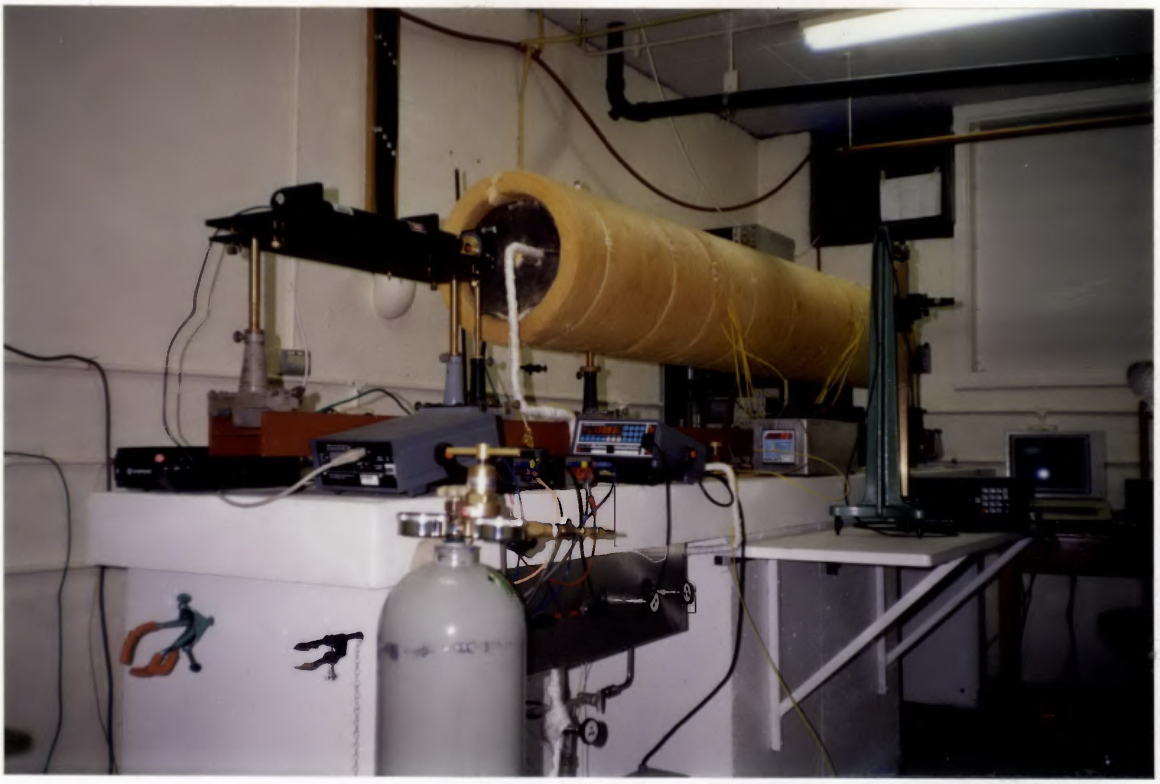

Plate 3.1 Right-side view of the field gradient birefringence experiment.

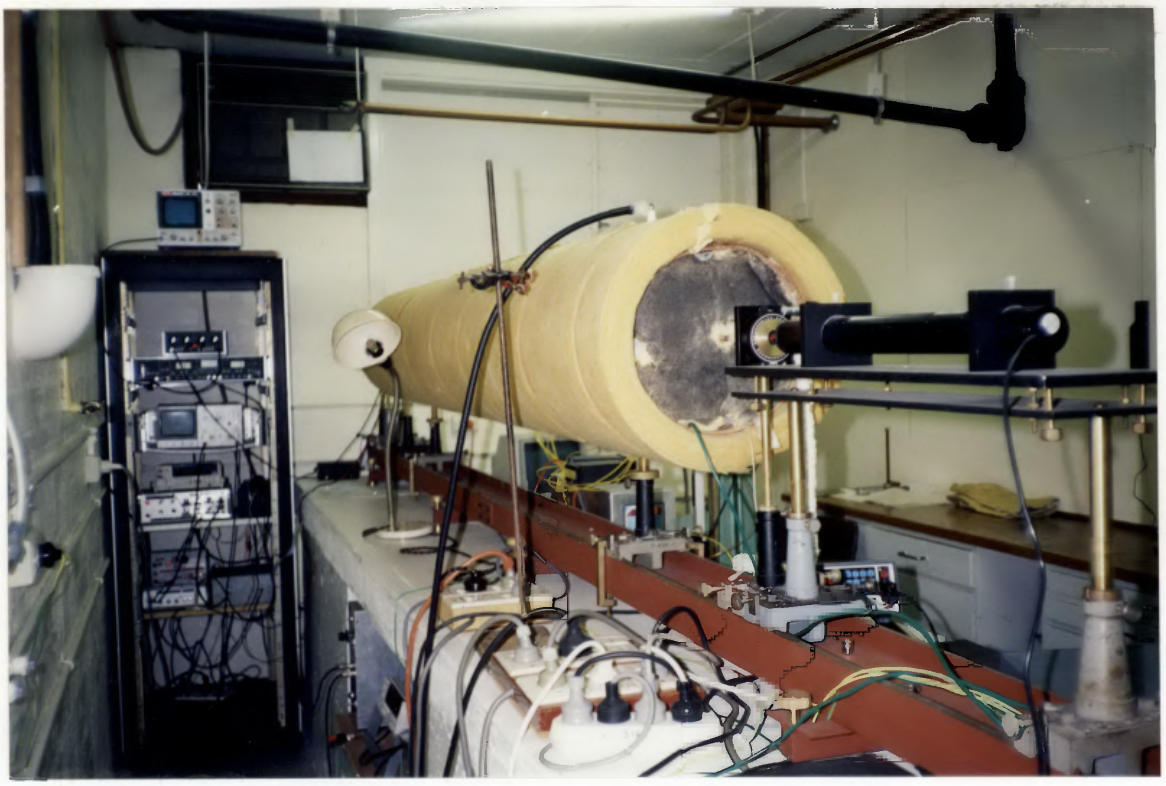

Plate 3.2 Left-side view of the field gradient birefringence experiment.

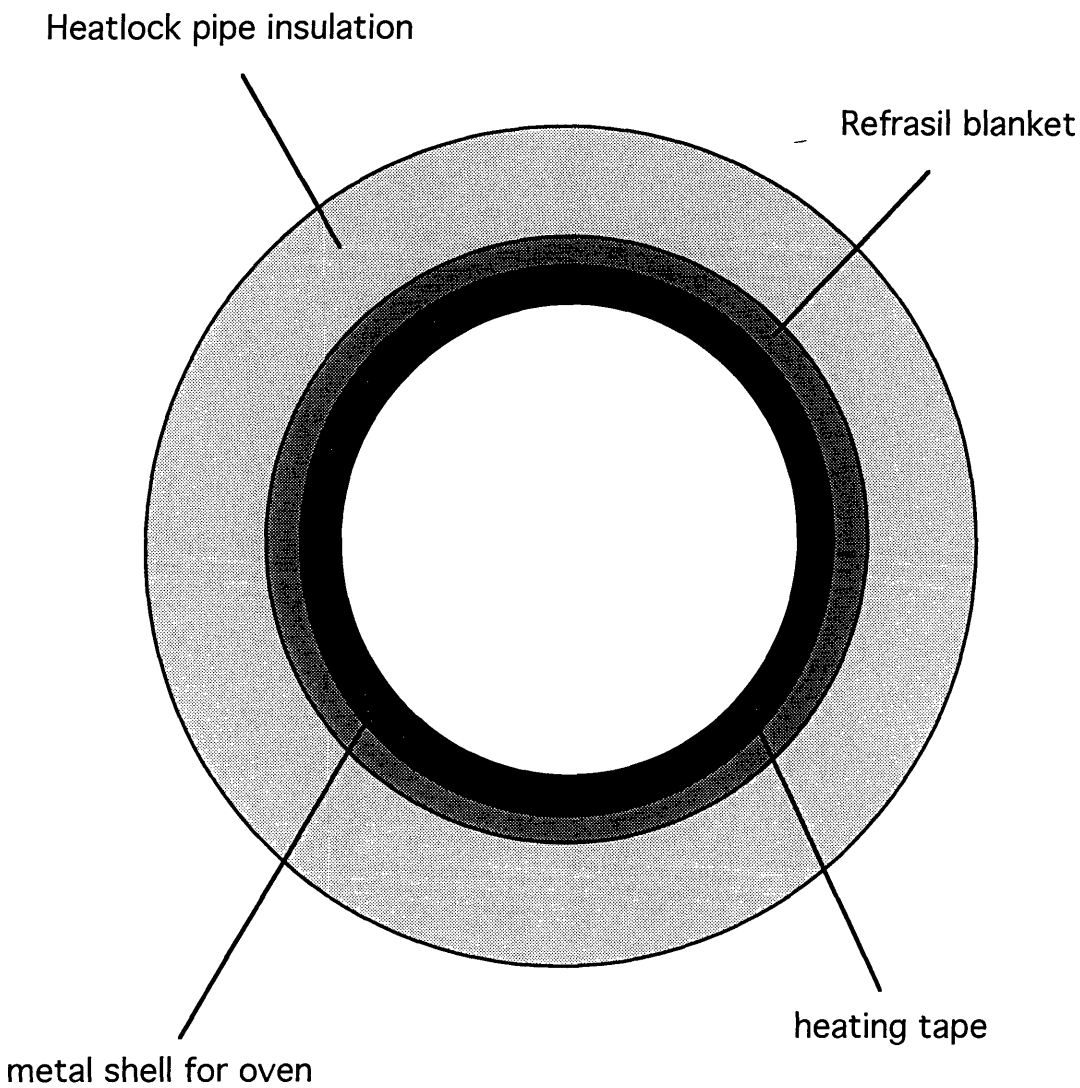

Figure 3.5 Cross section of the oven for the quadrupole cell.

where F_0 is the photon flux of the incident laser beam, Q is the quantum efficiency of detection and ΔT is the time interval of the measurement.

For a photomultiplier tube, Q is only about 8% at 632.8 nm, whereas the photodiode has Q of 80% and consequently a better signal/noise ratio should be obtained when using a photodiode.

After testing a 4 mm^2 photodiode (in place of the photomultiplier), operated in photovoltaic mode, using a high quality FET amplifier, the signal/noise ratio of the apparatus was found to have increased by at least an order of magnitude. Thus the photodiode was used as the detector for all the measurements performed in this study.

3.9 DETECTION SYSTEM

An automated detection system was designed for this apparatus in order to carry out the procedures outlined in section 2.3. The system, shown schematically in Figure 3.1, consists of a filter, lock-in amplifier, phase shifter, attenuator, power supply and computer.

The signal, after leaving the photodiode, passes along a 1 m length of coaxial cable, kept to a minimum length to minimize extraneous interference, to an Ithaco 4302 dual 24 db/octave filter. This filter is set up to operate with a high-pass filter with a cut-off frequency of 250 Hz and a low pass filter with a cut-off frequency of 500 Hz. With the reference signal from the sine-wave generator modulated at 389 Hz, the filter serves to eliminate any Kerr-effect signal at a frequency of 2ω that may arise from misalignment of the quadrupole cell. Also, any d.c. voltages are removed by operating the filter in the a.c. mode.

An EG&G Princeton Applied Research model 5209 lock-in amplifier is used to extract the desired modulated signal from the photodiode output voltage. This model also has several in-line filters that provide greater harmonic rejection. In this work, the bandpass filter was set to the reference frequency and used to further filter the signal. Depending on the signal/noise ratio of the experiment, a time constant of 3 s was usually used in conjunction with a sensitivity setting of 3 μV.

To ensure that the phase of the signal from the coil is in antiphase to the signal from the quadrupole cell, a phase shifter is used prior to the current supply of the coil. This process involves observing the signals from the two cells on an oscilloscope and adjusting the phase of the current entering the coil, so that the two signals cancel each other out. As a check, the automatic phase measurement facility on the lock-in amplifier is utilized to determine the phase of the signal from the coil which is then compared to that of the cell, the difference being 180° if the phases are properly set.

As the procedure for the experiment involved plotting the output of the lock-in amplifier as a function of the current through the Faraday coil, it was advantageous to use a programmable attenuator to control the current entering the coil from the power amplifier. The attenuator itself is controlled by a computer using a parallel interface.

The current passing through the coil for a particular setting of the attenuator is calculated by measuring the a.c. voltage across a 1000 Ω resistor in series with the Faraday coil. A Fluke 45 voltmeter, which has an accuracy of 0.2%, is used to measure the voltage. This arrangement is shown schematically in Figure 3.6.

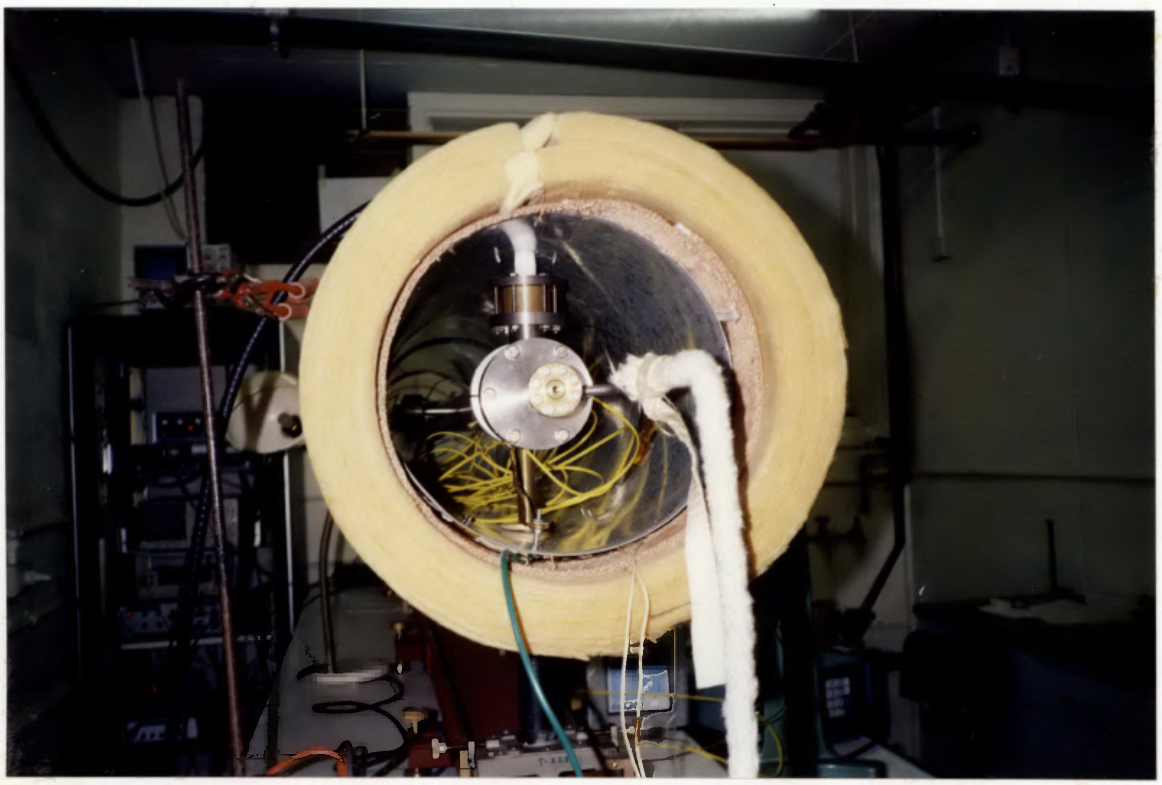

Plate 3.3 The gas quadrupole cell inside the oven.

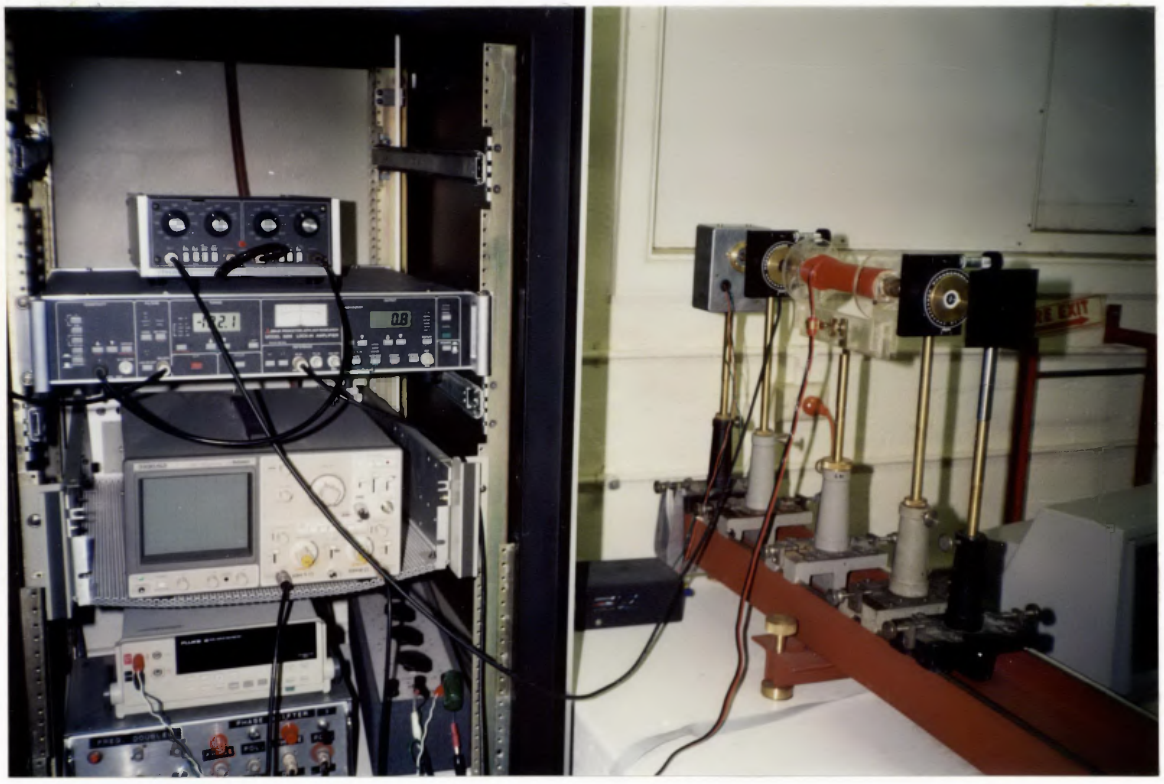

Plate 3.4 Some of the detection electronics and optical components.

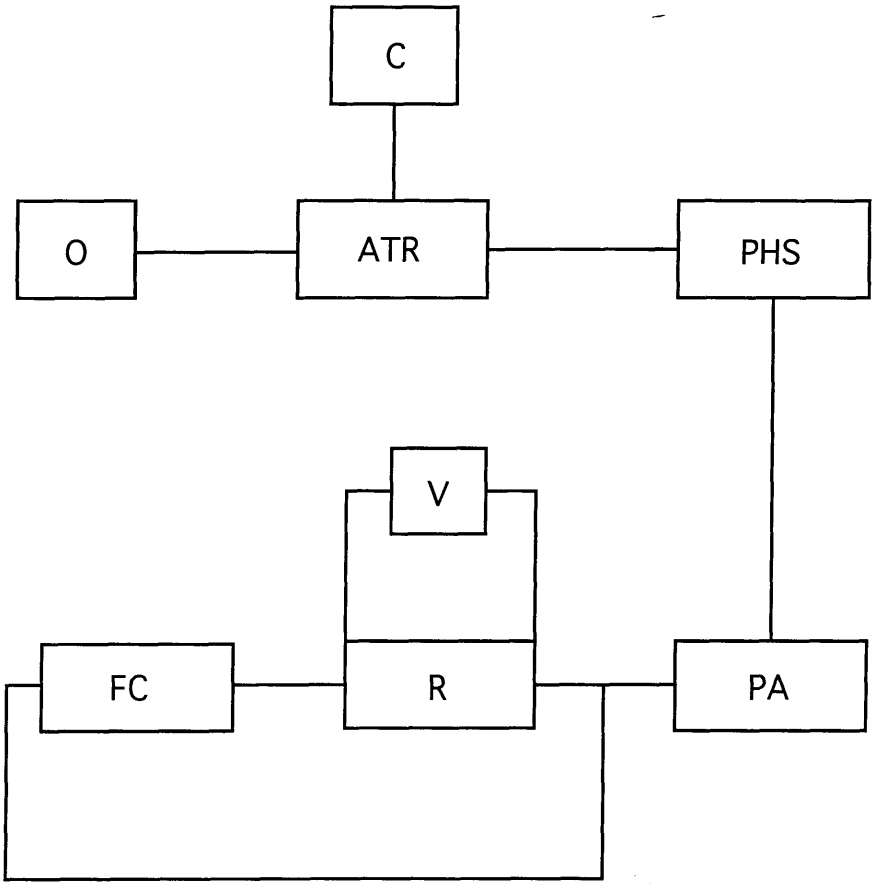

Figure 3.6 Arrangement used to provide and measure the nulling signal.

C, computer; O, oscillator; ATR, attenuator; PHS, phase shifter; PA, power amplifier; V, calibrated a.c. voltmeter; R, 1000 Ω resistor; FC, Faraday coil.

3.10 THE COMPUTER

An Apple IIe computer is used to control and collect data from the experiment during a measurement. With no commercially available software packages satisfying the requirements of the experiment, it was necessary to write a program in Applesoft Basic to perform the following tasks:

1) allow the operator to decide how many settings of the attenuator are to be used during any given run (a factor mainly determined by the signal/noise ratio);

2) communicate with the lock-in amplifier using a RS232 interface, enabling the computer to record and average a predetermined number of readings of the output from the lock-in amplifier, at specified time intervals, for a particular setting of the attenuator. A similar set-up with the Fluke voltmeter allows the computer to record the corresponding a.c. voltage across the 1000 Ω resistor. The program then prints the average output from the lock-in amplifier, together with the corresponding a.c. current through the coil, for each attenuator setting; and

3) change the setting of the attenuator to the next given value and wait a specified time before recommencing measurements. This allows the output of the lock-in amplifier to adjust to the shift in signal due to the change of current through the coil.

On the completion of the run, all the data points are plotted on a graph using commercially available computer software, so that the nulling current can be calculated.

3.11 PERFORMANCE OF THE DETECTION SYSTEM

Using five attenuator settings for each orientation of the quarterwave plate to obtain the null position, where each point is calculated from the average of 150 readings

($\approx$ 6 minutes) taken from the output of the lock-in amplifier (3 s time constant and 3 μV sensitivity), the limit of resolution of the experiment was determined to be $\approx 2 \times 10^{-9}$ rad.

Despite this excellent resolution, the accuracy of the final results depends on several possible systematic errors associated with the experiment. The main sources are the calibration of the Faraday coil (0.5%), calculation of the field gradient (1%), measurement of the pressure and temperature (0.5%) and alignment errors (1%). Thus, the values obtained for the quadrupole moment from this experiment, are estimated to have an uncertainty of at least $\pm$ 3%.

3.12 GAS HANDLING SYSTEM

As measurements of the field gradient induced birefringence were to be performed on gases and substances that are liquids or solids at room temperature, a gas-handling system capable of manipulating all types of compounds was designed and constructed for the apparatus. The system, shown schematically in Figure 3.7, is a simple network of stainless steel piping and valves joined by Swagelok fittings that provide a vacuum-tight seal. Glass traps link the gas handling system to a rotary vacuum pump with Cajon fittings.

The pressure in the quadrupole cell is monitored by either a Data Instruments low pressure transducer Model SA 25A (maximum pressure 170 kPa), or a Data Instruments high pressure transducer Model SA 500S (maximum pressure 3450 kPa). Both transducers provide an accuracy of better than 1% and, either can be selected using a simple two-way valve.

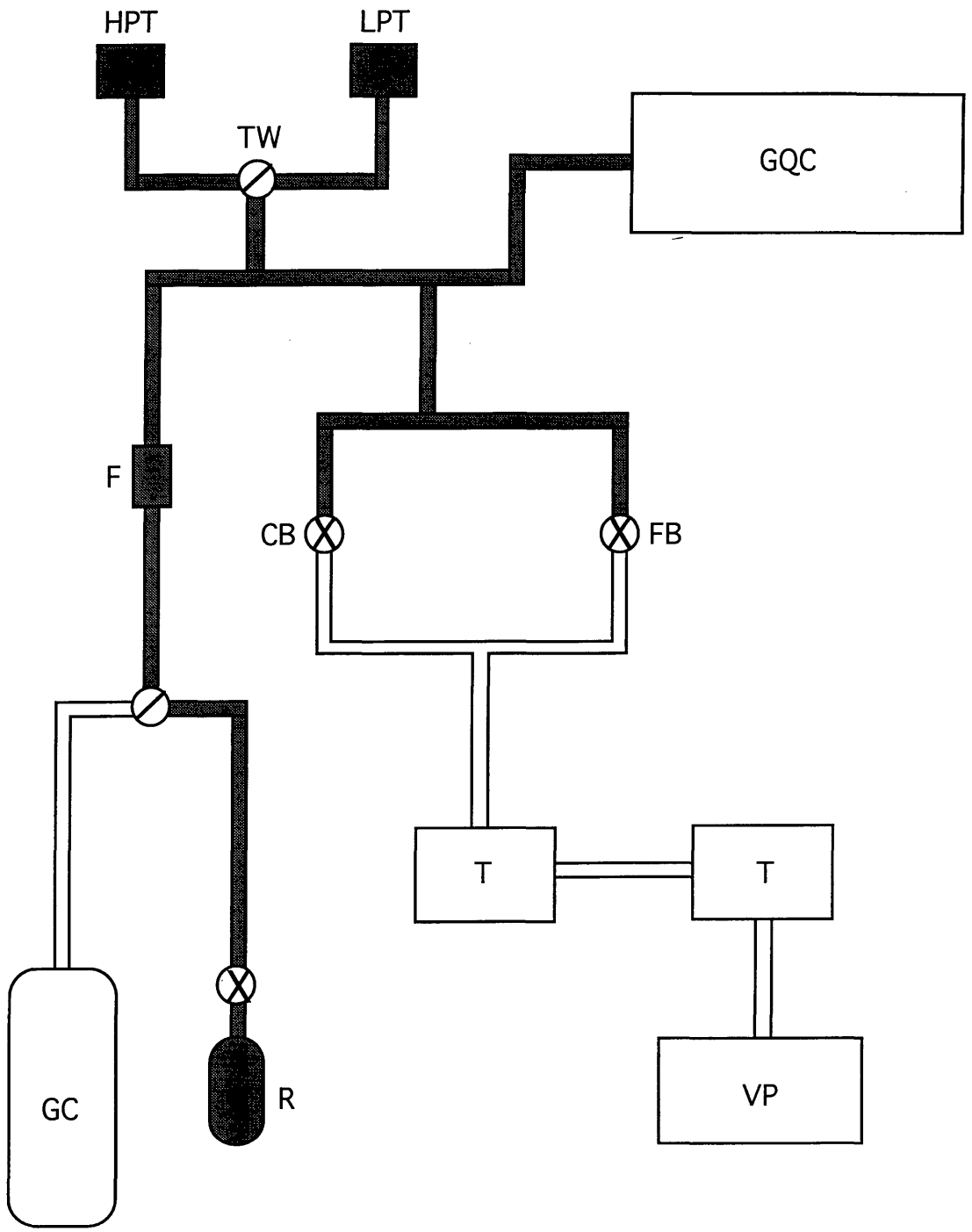

Figure 3.7 Gas handling system.

HPT, high pressure transducer; LPT, low pressure transducer; TW, two-way ball valve; GQC, gas quadrupole cell; F, filter; CB, coarse bellows valve; FB, fine bellows valve; GC, gas sample cylinder; R, solid and liquid reservoir; T, liquid nitrogen trap; VP, vacuum pump.

The filter (Swagelok model ss-4TF-0.05), with a pore size of 0.05 μm, served to remove dust from the samples before they entered the cell.

All the shaded components shown in Figure 3.7 are wrapped with electrical heating tape and fibreglass insulation tape, enabling the system to be heated to a maximum operating temperature of 100°C. Thus, pressures above the room temperature vapour pressure of the liquid can be used without condensation problems.

This system is very convenient as it allows the user to change from high-pressure gas applications to low-pressure vapour operations at elevated temperatures by simply manipulating several valves. The system is evacuated by a Metrovac rotary vacuum pump through a two-stage liquid nitrogen cold trap.

3.13 EXPERIMENTAL PROCEDURE

Initially, a small spirit level was used to make sure the optical rail was horizontal. The laser was then set in its mount and adjusted so that the beam was parallel to the rail.

The polarizer was then positioned on the rail and, using a reference polarizer (azimuth 45 ± 1°) and a power meter to monitor the light intensity, rotated until the transmission axis of the polarizer coincided with that of the reference. This allowed the azimuth to be set within 5×10^{-6} rad using the precision rotator.

Using a Faraday coil to modulate the signal, as shown in Figure 3.8, the analyzer was then inserted and crossed with respect to the polarizer such that the output

from the lock-in amplifier was zero. Next, the quarterwave plate was inserted between the polarizer and Faraday coil and nulled photometrically so that its azimuth was 45°.

The quadrupole cell was then set in position inside the oven, with the plane of the wires vertical relative to the optical rail. The thermocouples were attached to the respective sites located along the length of the cell. Simple rotation of the cell allowed the azimuth to be set to $0 \pm 1°$. Split rings clamped the quadrupole cell in position.

Ground-loop errors were eliminated by correct grounding procedures, thereby minimizing common mode interference and ensuring operator safety.

Figure 3.8 Arrangement used for the alignment of the analyzer.

3.14 CALIBRATION OF THE FARADAY COIL

Treating the Faraday coil as an ideal circular retarder, the Faraday rotation is given by the expression

$$\theta = VHl = K_F i \tag{3.2}$$

where V is the Verdet constant of water, H is the magnetic field strength, l is the length of the core, K_F is the calibration constant of the coil and i is the solenoid current. As the null condition depends on K_F, an accurate determination of this constant is required.

The Faraday coil was calibrated using the experimental arrangement shown in Figure 3.9. This involved applying currents of up to 1.8 A d.c. to the coil and nulling the static rotation manually with the analyzer. After averaging a series of measurements, the calibration constant was found to be

$$K_F = 0.6215 \pm 0.0056 \quad \mu\text{rad mA}^{-1}$$

Periodic checks over several months showed no significant drift (<1%) from this value.

3.15 MEASUREMENT

In order to separate the hyperpolarizability and orientational terms, a temperature-dependence study is required. In addition, as molecular interactions may contribute significantly to the observed birefringence, it is necessary to perform pressure-dependence studies to properly account for these interactions, thereby enabling reliable values for the free-molecule properties to be obtained.

Preliminary experiments carried out on carbon dioxide and nitrogen, using gas pressures ranging from 200 – 2500 kPa, revealed no pressure dependence of ${}_{m}Q$ at room temperature. Hence, measurements of ${}_{m}Q$ at any given temperature were usually made at the one pressure, reducing any strain effects in the windows due to pressure changes. Before measurements on each new compound were started, a calibration with carbon dioxide was performed. This value was then compared to the standard result obtained from the investigation of the temperature dependence of the field gradient birefringence effect presented later in Chapter 4. If the result varied by more than 2% from the reference value, then the fault, either in the optical or electrical components of the apparatus, was sought and corrected before proceeding with measurements.

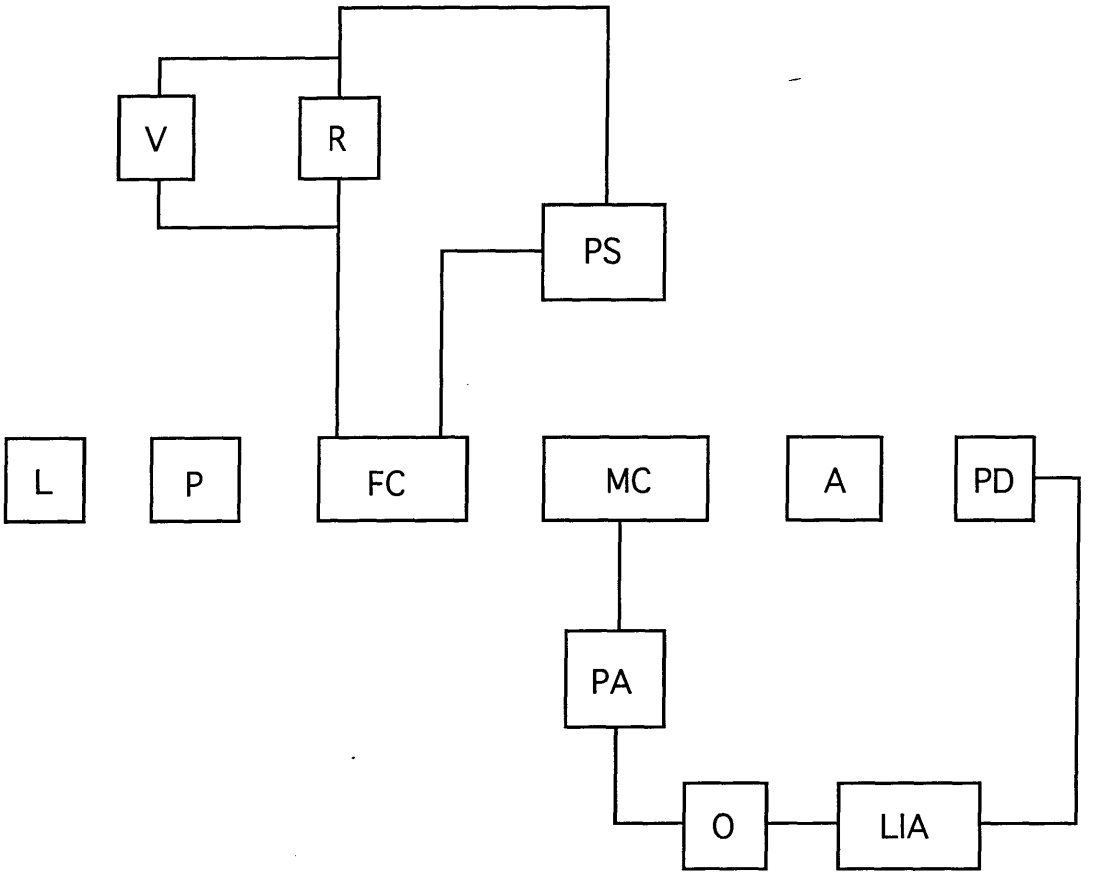

Figure 3.9 Calibration of the Faraday coil by rotation of the analyzer.

L, laser; P, polarizer; FC, Faraday coil; MC, modulating coil; A, analyzer; PD, photodiode; V, d.c. voltmeter; R, 10 Ω resistor; PS, d.c. power supply; LIA, lock-in amplifier; O, oscillator; PA, power amplifier.

The cell was evacuated for ten minutes before being filled with the gas. A maximum gas pressure of ≈ 1800 kPa was chosen, so that the expression for the field gradient induced birefringence,[2] based on low gas densities, was still valid.

If the sample to be studied was a liquid at room temperature, it was degassed by three freeze-pump-thaw cycles prior to use. For any particular measurement, the pressure never exceeded 3/4 of the equilibrium vapour pressure at the given temperature. Any uncertainty in the measurements due to impurities in the samples is considered to be negligible, as all the samples studied were analyzed using gas chromatography and were found to have a purity of > 99%.

From the mean temperature and pressure readings, the molar volume, V_m, was calculated using published virial coefficients [3] and the virial equation

$$p = \frac{RT}{V_m}\left(1 + \frac{B}{V_m} + \frac{C}{V_m^2} + \ldots\right) \tag{3.3}$$

The filling of the cell was always carried out the night before the measurements were made to allow 1) the system to equilibrate at the particular temperature and 2) the windows of the quadrupole cell to stabilize to the induced strain resulting from the pressurizing of the cell.

As it was necessary to disassemble the apparatus at various stages of this project, it was reassuring that the experiment could be reassembled and realigned to give ${}_mQ$ for carbon dioxide at room temperature to within 1%.

The results presented in the following chapters were obtained using the apparatus and procedures described in these sections.

3.16 REFERENCES

1. D.P. Shelton and R.E. Cameron, *Rev. Sci. Instrum.*, **59**, 430 (1988).

2. A.D. Buckingham, *J. Chem. Phys.*, **30**, 1580 (1959).

3. J.H. Dymond and E.B. Smith, *The Virial Coefficients of Pure Gases and Mixtures* (Clarendon Press, Oxford, 1980).